Surv Geophys (2016) 37:529–556
DOI 10.1007/s10712-016-9360-8

Assessing and Improving Land Surface Model Outputs Over Africa Using GRACE, Field, and Remote Sensing Data

Mohamed Ahmed[1,2] · Mohamed Sultan[1] · Eugene Yan[3] · John Wahr[4]

Received: 13 October 2015 / Accepted: 19 January 2016 / Published online: 8 February 2016

Abstract The Gravity Recovery and Climate Experiment (GRACE), along with other relevant field and remote sensing datasets, was used to assess the performance of two land surface models (LSMs: CLM4.5-SP and GLDAS-Noah) over the African continent and improve the outputs of the CLM4.5-SP model. Spatial and temporal analysis of monthly (January 2003–December 2010) Terrestrial Water Storage (TWS) estimates extracted from GRACE (TWS_{GRACE}), CLM4.5-SP ($TWS_{CLM4.5}$), and GLDAS-Noah (TWS_{GLDAS}) indicates the following: (1) compared to GRACE, LSMs overestimate TWS in winter months and underestimate them in summer months; (2) the amplitude of annual cycle (AAC) of TWS_{GRACE} is higher than that of TWS_{LSM} (AAC: $TWS_{GRACE} > TWS_{GLDAS} > TWS_{CLM4.5}$); (3) higher, and statistically significant correlations were observed between TWS_{GRACE} and TWS_{GLDAS} compared to those between TWS_{GRACE} and $TWS_{CLM4.5}$; (4) differences in forcing precipitation and temperature datasets for GLDAS-Noah and CLM4.5-SP models are unlikely to be the main cause for the observed discrepancies between TWS_{GRACE} and TWS_{LSM}; and (5) the CLM4.5-SP model overestimates

✉ Mohamed Sultan
mohamed.sultan@wmich.edu

Mohamed Ahmed
mohamed.ahmed@wmich.edu

Eugene Yan
eyan@anl.gov

John Wahr
wahr@lemond.colorado.edu

[1] Department of Geosciences, Western Michigan University, 1903 West Michigan Avenue, Kalamazoo, MI 49008, USA

[2] Department of Geology, Faculty of Science, Suez Canal University, Ismailia 41522, Egypt

[3] Environmental Science Division, Argonne National Laboratory, 9700 South Cass Avenue, Argonne, IL 60439, USA

[4] Department of Physics, University of Colorado at Boulder, 2000 Colorado Avenue, Boulder, CO 80309, USA

evapotranspiration (ET) values in summer months and underestimates them in winter months compared to ET estimates extracted from field-based (FLUXNET-MTE) and satellite-based (MOD16 and GLEAM) ET measurements. A first-order correction was developed and applied to correct the CLM4.5-derived ET, soil moisture, groundwater, and TWS. The corrections improved the correspondence (i.e., higher correlation and comparable AAC) between $TWS_{CLM4.5}$ and TWS_{GRACE} over various climatic settings. Our findings suggest that similar straightforward correction approaches could potentially be developed and used to assess and improve the performance of a wide range of LSMs.

Keywords GRACE · GLDAS-Noah · CLM4.5-SP · TWS · Evapotranspiration · Africa

1 Introduction

The twin Gravity Recovery and Climate Experiment (GRACE) satellite mission is a joint project between National Aeronautics and Space Administration (NASA) in the USA and German Aerospace Center (DLR) in Germany. GRACE was launched on March 17, 2002, to map: (1) the temporal variations in Earth's global gravity field on a monthly basis with unprecedented accuracy and (2) Earth's static gravity field with orders of magnitude higher accuracy than those obtained from previous satellite missions (Tapley et al. 2004). The variability in gravity field solutions mapped by the GRACE satellite is directly related to the redistribution of mass at or near the Earth's surface. The largest signals observable in the GRACE data are coming from spatial and temporal variations in terrestrial water storage (TWS) (Wahr et al. 1998). TWS refers to the total vertically integrated water content in an area regardless of the reservoir (surface water, groundwater, soil moisture and permafrost, snow and ice, or wet biomass) in which it resides.

Recent applications of GRACE data have resulted in advances in various disciplines (Wouters et al. 2014) including hydrology (Rodell et al. 2009; Ahmed et al. 2011, 2014; Famiglietti et al. 2011; Sultan et al. 2013, 2015), oceanology (e.g., Jacob et al. 2012; Gardner et al. 2013), cryosphere (e.g., Velicogna and Wahr 2013; Velicogna et al. 2014), and solid Earth fields (e.g., Steffen and Wu 2011; Han et al. 2013). However, such applications are hampered by the relatively low horizontal resolution of GRACE data and by the fact that GRACE does not have vertical resolution (e.g., Wahr et al. 2004, 2006). In other words, GRACE cannot distinguish between anomalies resulting from different compartments (e.g., surface water, groundwater, soil moisture, snow, and biomass) of TWS. The integration of land surface models (LSMs) outputs with GRACE-derived TWS (TWS_{GRACE}) data is now providing opportunities to: (1) extract individual components, such as soil moisture and groundwater, from TWS_{GRACE} estimates and (2) improve the horizontal resolution of TWS_{GRACE} data. Examples of efforts that utilized LSMs outputs to improve the horizontal and vertical resolutions of TWS_{GRACE} include the use of Global Land Data Assimilation System (GLDAS) (Rodell et al. 2004), the Community Land Model (CLM) (Lawrence et al. 2011), and the WaterGAP Hydrological Model (WGHM) (Döll et al. 2003, 2014a, b).

Scaling techniques were recently used to extrapolate the TWS_{GRACE} estimates from their effective spatial resolution (a few hundred kilometers) to finer spatial scales ($\sim$100 km); in this approach, GLDAS-derived (TWS_{GLDAS}) and CLM-derived TWS (TWS_{CLM}) estimates were used to develop a multiplicative gain factors to rescale

TWS_{GRACE} (Landerer and Swenson 2012). Scaling factors results based on six (GLDAS-Noah, GLDAS-Mosaic, GLDAS-VIC, GLDAS-CLM2, CLM4.0, and WGHM) LSMs were compared over 60 watersheds; similarities over humid, sub-humid, and high-latitude regions were observed, yet large differences were found over arid and semiarid basins and intensively irrigated areas (Long et al. 2015).

Various attempts were made to use LSM outputs to improve the vertical resolution of TWS_{GRACE}. For example, GLDAS model was used to estimate the contributions of TWS compartments (e.g., soil moisture and snow water equivalent) to TWS_{GRACE} for the purpose of quantifying modern recharge in the North-Western Sahara Aquifer System (Gonçalvès et al. 2013) and estimating depletion rates of aquifer systems in the Middle East (Voss et al. 2013), northern China (Feng et al. 2013), northern India (Rodell et al. 2009; Chen et al. 2014), California (Scanlon et al. 2012), and Turkey (Lenk 2013). Similarly, the CLM model was used to estimate the contributions of soil moisture, canopy, snow, and river channel storages to TWS_{GRACE} and to quantify the depletion rates of aquifer systems in northern India (Tiwari et al. 2009) and in the Middle East (Joodaki et al. 2014).

It is worth mentioning that the overwhelming majority of recent applications to improve the vertical resolution of GRACE data over Africa utilized outputs of GLDAS-Noah and CLM models (e.g., Gonçalvès et al. 2013). There are several problems with such applications. For instance, none of these LSMs (e.g., GLDAS and CLM) are calibrated against field measurements and/or observations, nor can they account for anthropogenic contributions or simulate dynamic lakes or reservoirs. Additional problems include: The GLDAS model does not simulate groundwater and river channel storages (Rodell et al. 2004), and the CLM model overestimates evapotranspiration (ET) and does not adequately simulate the partitioning of ET into soil evaporation, canopy evaporation, and transpiration (Schaefer et al. 2012; Hudiburg et al. 2013; Tang and Riley 2013; Swenson and Lawrence 2014).

Given the fact that GRACE measures both natural (climatic) and anthropogenically induced variations in TWS, one would expect a general correspondence between TWS_{GRACE} and LSM-derived TWS (TWS_{LSM}) in hydrologic systems that are largely controlled by natural variations. In a recent study, we investigated the nature (climatic and/or human pressure-related) of the factors controlling the observed variations of TWS_{GRACE} across all the major hydrologic systems in Africa and identified the basins that are largely controlled by natural factors (Ahmed et al. 2014).

In this paper, we select four of the previously investigated African hydrologic systems (Niger, Okavango, Zambezi, and Limpopo basins) that are least affected by anthropogenic practices and are largely controlled by natural factors. We first demonstrate that for those four basins there are discrepancies between TWS_{GRACE} and TWS_{LSM}; then, we investigate whether these observed discrepancies are largely related to differences in model forcing inputs (e.g., precipitation and temperature) and/or due to differences in the adopted algorithms, and finally, we apply first-order corrections to improve the outputs of LSMs and the correspondence between TWS_{GRACE} and TWS_{LSM}. We also show that the adopted corrections can improve the correspondence between TWS_{GRACE} and TWS_{LSM} across the entire African continent. By improving the outputs of the LSMs and applying approaches similar to those listed above (e.g., Tiwari et al. 2009; Landerer and Swenson 2012; Joodaki et al. 2014), one can better refine the vertical and horizontal resolution of TWS_{GRACE}.

Unlike many of the previous and ongoing attempts (e.g., Reichle et al. 2002; Walker et al. 2003; Niu and Yang 2006; Moradkhani 2008; Zaitchik et al. 2008; Werth et al. 2009; Werth and Güntner 2009; Widiastuti 2009; Oleson et al. 2010; Su et al. 2010; Gent et al. 2011; Forman et al. 2012; Houborg et al. 2012; Lawrence et al. 2012; Li et al. 2012; Awange et al.

2014; Eicker et al. 2014; Swenson and Lawrence 2014) that utilize TWS_{GRACE} data to assess and improve the performance and/or the outputs of LSMs, our approach does not require access to extensive computational resources required to simulate LSMs' outputs.

2 Data and Methodology

In this section, we briefly describe the GRACE and LSM datasets, procedures used to derive TWS_{GRACE}, TWS_{LSM} and related products, and the independent ET datasets that were used to assess and improve the performance of LSM simulations. All of the data used in this exercise are monthly datasets and were acquired throughout the time period of January 2003–December 2010.

2.1 GRACE-Derived TWS Data (TWS_{GRACE})

We analyzed level 2 GRACE gravity field solutions [Release 05 (RL05)] from the GRACE database provided by the University of Texas Center for Space Research (available at ftp://podaac.jpl.nasa.gov/allData/grace/L2/CSR/RL05; last access: October 2015). These solutions are represented in terms of fully normalized spherical harmonic decompositions up to degree and order of 60. The time-variable component of the gravity field was obtained by removing the long-term mean of the Stokes coefficients from each of the monthly values. Generally, errors in the GRACE-derived gravity field coefficients are categorized as systematic and random errors. The systematic errors, which are correlated within a particular spectral order, were reduced by applying destriping filters developed by Swenson and Wahr (2006). The random errors, which increase as a function of spherical harmonic spectral degree (Wahr et al. 2006), were minimized by applying a Gaussian filter with a half-width corresponding to 200 km (Wahr et al. 1998). The spherical harmonic coefficients were then converted to mass (TWS_{GRACE}) grids ($1^\circ \times 1^\circ$) of equivalent water thickness following the procedures described by Wahr et al. (1998). The temporal gaps in TWS_{GRACE} data, associated with battery-related power limitations, were filled using linear interpolation techniques of the previous and the following months.

The peak-to-peak amplitude of annual cycle (AAC) image was generated by simultaneously fitting an annual and semiannual sine and cosine, mean, and linear trend for each grid point in the TWS_{GRACE} time series. The seasonality differences in TWS_{GRACE} data were examined by calculating the difference between the TWS_{GRACE} of the boreal spring months (March, April, and May) and the boreal fall months (September, October, and November).

The uncertainty (1-sigma) associated with TWS_{GRACE} estimates, averaged over a basin, was calculated by: (1) simultaneously fitting and removing an annual and semiannual sine and cosine, mean, and linear trend to estimate monthly TWS_{GRACE} residuals and (2) calculating the standard deviation of the monthly TWS_{GRACE} residuals. The calculated uncertainty is conservative, given that the variabilities from the short-time and inter-annual periods were included; by including those non-normally distributed variabilities, the uncertainty could be overestimated (Wahr et al. 2006; Klees et al. 2007). The calculated uncertainty was used to examine the statistical significance of the differences between the TWS_{GRACE} and TWS_{LSM}; if the difference between the TWS_{GRACE} and TWS_{LSM} for any month was larger than the value of 1-sigma, we can be 68.3 % confident that difference is statistically significant and that the value of the TWS_{LSM} need to be corrected (Wahr 2007; Swenson and Lawrence 2014).

The Nash–Sutcliffe efficiency (NSE) coefficient was used to calculate the degree of statistical agreement between the TWS_{GRACE} and the TWS_{LSM}. NSE is a normalized statistical approach that indicates how well the plot of observed versus simulated data fits the 1:1 line relationship (Nash and Sutcliffe 1970). The NSE coefficient is calculated using the following equation:

$$\mathrm{NSE} = 1 - \frac{\sum_{i=1}^{n}(O_i - S_i)^2}{\sum_{i=1}^{n}(O_i - \bar{O})^2} \quad (1)$$

where O_i is the observed value (TWS_{GRACE}), S_i is the simulated value (TWS_{LSM}), n is the number of measurements, and $\bar{O}$ is the average of O_i over the entire period (January 2003–December 2010). The optimal value for the NSE is equal to 1.0. The NSE coefficient was used to examine the correspondence between temporal datasets other than GRACE such as precipitation, temperature, and ET.

2.2 Land Surface Models TWS Outputs (TWS_{LSM})

The outputs of two LSMs were used in this study: the TWS outputs of the GLDAS-Noah and the CLM4.5-SP models. To unify the spatial resolution of TWS_{GRACE} and TWS_{LSM}, the LSM grids were converted to spherical harmonics coefficient (degree/order of 60), the long-term mean was removed, and residuals were filtered using filters (destriping and Gaussian) applied to GRACE data and then converted to mass grids. The AAC and the seasonality difference images of the TWS_{LSM} were calculated using the procedures described for TWS_{GRACE}. As described above, TWS_{GRACE} was compared to TWS_{LSM}.

2.2.1 GLDAS Model TWS Outputs (TWS_{GLDAS})

The GLDAS is a NASA land surface modeling system that integrates the global satellite-based measurements to drive advanced simulations for climatic and hydrologic investigations (Rodell et al. 2004). The GLDAS forcing precipitation data are extracted from the National Oceanic and Atmospheric Administration (NOAA) and Climate Prediction Center (CPC) Merged Analysis of Precipitation (CMAP) (Xie and Arkin 1997). GLDAS simulates TWS as the summation of soil moistures, snow, and canopy storages through four main land surface models: VIC (Liang et al. 1996), Noah (Koren et al. 1999), MOSAIC (Koster and Suarez 1996), and CLM (Dai et al. 2003). The TWS_{GLDAS} was extracted from the GLDAS version 1 Noah model (spatial resolution: 1° × 1°; available at: ftp://hydro1.sci.gsfc.nasa.gov; last access: October 2015).

2.2.2 CLM Model TWS Outputs (TWS_{CLM})

CLM is the land component of the Community Earth System Model (CESM) (Gent et al. 2011; Lawrence et al. 2011; Hurrell et al. 2013). CLM simulates the partitioning of mass and energy from the atmosphere and the redistribution of mass and energy within the land surface. The CLM [version 4.5 satellite phenology (SP)] simulations used in this study are forced with atmospheric conditions for the period 1850–2010 extracted from the Climate Research Unit, National Centers for Environmental Prediction (CRUNCEP) (Viovy and Ciais 2015) datasets. Components of TWS outputs from the CLM4.5 model (spatial resolution: 1.25° longitude × 0.9° latitude) include soil moisture, snow, vegetation canopy

storage, channel storage in rivers, and unconfined aquifer storage. CLM4.5 products are available at: https://www.earthsystemgrid.org (last access: October 2015).

2.3 Evapotranspiration (ET) Data

Three main independent ET datasets were used in this study: two satellite-based ET estimates [the Moderate Resolution Imaging Spectroradiometer (MODIS-MOD16) and the Global Land Evaporation Amsterdam Methodology (GLEAM)] and one field-based ET estimate [FLUXNET-Model Tree Ensembles (MTE)]. The term "measurement-based ET ($ET_{measured}$)" was used throughout this study to denote both satellite-based and field-based ET estimates. $ET_{measured}$ values were used to validate the LSM-derived ET (ET_{LSM}) estimates and to correct the bias in them, if any. ET datasets were gridded at 0.5° × 0.5° to unify the spatial resolution of different ET products. The AAC images and the uncertainty bounds were calculated using the procedures described above for TWS_{GRACE}. As in the case of the TWS_{GRACE} and TWS_{LSM}, the NSE coefficients were calculated between the $ET_{measured}$ estimates and the model-based ET estimates (ET_{LSM}).

2.3.1 MODIS-MOD16 ET Data (ET_{MOD16})

The MOD16 algorithm computes global potential and actual ET for vegetated land areas at a spatial resolution of one square kilometer and at varying temporal resolutions (8 days, monthly, annual intervals) (Mu et al. 2007). MOD16 uses MODIS land cover, albedo, Leaf Area Index, an enhanced vegetation index, and a daily meteorological reanalysis data set from NASA's Global Modeling and Assimilation Office (GMAO) as inputs for regional and global evaporation estimation applying the Penman–Monteith method (Mu et al. 2011). The MOD16 data used in this study are available at ftp://ftp.ntsg.umt.edu/pub/MODIS/NTSG_Products/MOD16 (last access: October 2015).

2.3.2 Global Land Evaporation Amsterdam Methodology (GLEAM) ET Data (ET_{GLEAM})

GLEAM is a set of algorithms driven by satellite observations that estimates different components of ET (transpiration, interception loss, bare soil evaporation, snow sublimation, and open water evaporation) (Miralles et al. 2011b). GLEAM provides global daily estimates of ET with a spatial resolution of 0.25° × 0.25°. GLEAM version 2B, used in this study (available at: http://foofoo.ugent.be/satex/GLEAM/; last access: October 2015), is forced by CPC MORPHing technique (CMORPH) precipitation data, WAter Cycle Multi-mission Observation Strategy-Climate Change Initiative (WACMOS-CCI) surface soil moisture data, NASA Land Parameter Retrieval Model (NASA-LPRM) vegetation optical depth data, Clouds and Earth's Radiant Energy System-SYNoptic radiative fluxes and clouds version 1 (CERES-SYN1) degradation flux data, Atmospheric Infrared Sounder (AIRS) version 7 air temperature data, and Global Snow Monitoring for Climate Research (GlobSnow) snow water equivalents data (Miralles et al. 2011a, b). GLEAM uses a modified Priestley and Taylor model in combination with an evaporative stress module and a Gash analytical model of rainfall interception to derive evaporation (Miralles et al. 2010).

2.3.3 FLUXNET-MTE ET Data ($ET_{FLUXNET}$)

The FLUXNET network of eddy covariance towers applies the MTE approach to provide global, gridded (0.5° × 0.5°), monthly (starting from January 1982) estimates of sensible and latent heat and carbon fluxes (available at: https://www.bgc-jena.mpg.de/geodb/projects/Home.php; last access: October 2015). FLUXNET-MTE uses a machine-learning algorithm to estimate the surface–atmosphere fluxes from a suite of explanatory variables describing meteorological and land surface conditions (Jung et al. 2011). The MTE was trained using eddy covariance observations from individual FLUXNET facilities (number of flux towers in 2014: 683) and then applied at the global scale. In this study, ET values were extracted from FLUXNET-MTE latent heat flux estimates by multiplying these estimates by the inverse of the latent heat of vaporization.

2.4 Model Forcing Rainfall (R) and Temperature (T) Data

To check whether differences between TWS_{GRACE} and TWS_{LSM} if any are related to differences in LSM input data, the forcing data for the LSMs were compared spatially in a Geographic Information System (GIS) environment and temporally (time series analyses) to one another. Precipitation and temperature were found to be the primary forcing parameters over most of the African continent, while specific humidity, wind speed, surface pressure, and solar radiation played a secondary role (e.g., Bucchignani et al. 2015). In this study, the primary LSM forcing parameters (precipitation and temperature) were investigated. If we were to observe large variations in the degree to which TWS_{GRACE} corresponds to each of TWS_{GLDAS} and $TWS_{CLM4.5}$ and if these variations were related to differences in model inputs, one would expect to observe large variations in these inputs. For time series analysis, the temporal mean was removed from each of the forcing datasets. The uncertainty bounds were calculated using the procedures described above for TWS_{GRACE}. As in the case of the TWS_{GRACE} and TWS_{LSM}, the NSE coefficients were calculated between CLM4.5 and GLDAS forcing precipitation and temperature measurements.

3 Assessing the Performance of LSMs

3.1 LSMs-Derived TWS

Figure 1 shows the peak-to-peak AAC over the African continent that was generated from GLDAS (TWS_{GLDAS}; Fig. 1a), GRACE (TWS_{GRACE}; Fig. 1b), and CLM4.5 ($TWS_{CLM4.5}$; Fig. 1c) TWS data over the investigated period of January 2003–December 2010. Examination of Fig. 1 shows that the highest annual amplitude of TWS over Africa occurs over areas affected by the Intertropical Convergence Zone (ITCZ). The ITCZ (latitude domain: 23.4°N to 23.4°S) is characterized by low pressure, trade wind convergence and confluence, increased cloudiness, high surface temperature, and high rainfall. The January and July locations of the ITCZ are shown in Fig. 1. Inspection of the AAC images over the African continent shows similarities in patterns between TWS estimates extracted from GRACE, GLDAS, and CLM4.5, but differences in magnitude (AAC: $TWS_{GRACE} > TWS_{GLDAS} > TWS_{CLM4.5}$). Those differences are maximized in areas experiencing the highest annual amplitude of TWS, the areas affected by ITCZ (Fig. 1).

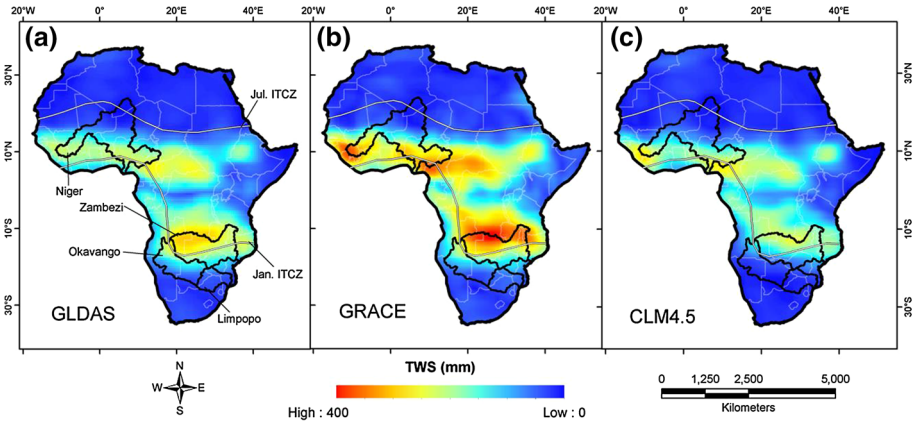

Fig. 1 Peak-to-peak amplitude of annual cycle (AAC: in mm) from **a** TWS_{GLDAS}, **b** TWS_{GRACE}, and **c** $TWS_{CLM4.5}$ over the African continent during the period from January 2003 to December 2010. Also shown are the January and July positions of the ITCZ (Levin et al. 2009) and the spatial distribution of the investigated watersheds

Examination of Fig. 1 and Table 1 reveals that the CLM4.5 model underestimates the amplitude of the seasonal cycle of TWS compared to that extracted from GLDAS and GRACE. In the Niger Basin, the AAC for TWS_{GRACE}, TWS_{GLDAS}, and $TWS_{CLM4.5}$ is estimated at 181 ± 10, 135, and 130 mm, respectively; in the Zambezi Basin, they are 310 ± 42, 266, and 213 mm, respectively. In the Limpopo and Okavango basins, the AAC of TWS_{GRACE} is twice as large as that of the $TWS_{CLM4.5}$ (Limpopo Basin: GRACE: 71 ± 26 mm; GLDAS: 69 mm; CLM4.5: 29 mm; Okavango Basin: GRACE: 134 ± 21 mm; GLDAS: 126 mm; CLM4.5: 57 mm).

Figure 2 compares the seasonality differences in TWS_{GRACE} and TWS_{LSM}. Examination of Fig. 2 shows dipolar patterns across the equator, negative, and positive polarities in the northern and southern hemispheres, respectively. Those patterns are largely controlled by ITCZ-related migration of monsoonal winds from south of the equator in boreal winter to north of the equator in boreal summer (Gent et al. 2011). The dipolar features of TWS_{GRACE}, TWS_{GLDAS}, and $TWS_{CLM4.5}$ are similar in patterns, but differ in magnitude (seasonality difference: $TWS_{GRACE} > TWS_{GLDAS} > TWS_{CLM4.5}$).

Time series for the selected watersheds are displayed in Fig. 3. In Fig. 3a–d, the correspondence between the TWS_{GRACE} and TWS_{CLM} (NSE: GRACE/CLM4.5) and between TWS_{GRACE} and TWS_{GLDAS} (NSE: GRACE/GLDAS) values are displayed in the upper right (blue text) and the lower right (red text) corners, respectively. Inspection of Fig. 3 shows varying degrees of correspondence in patterns, phases, and magnitudes between the measured (TWS_{GRACE}) and modeled (TWS_{LSM}) estimates of TWS. Figure 3 shows that the CLM4.5 model overestimates TWS in winter months and underestimates them in summer months compared to TWS_{GRACE}. For the Niger (Fig. 3a) and the Zambezi (Fig. 3b) basins, the patterns and phases are quite similar, yet the difference between each of the TWS_{LSM} and the TWS_{GRACE} exceeds TWS_{GRACE} uncertainty bounds. The correspondence between the TWS_{GRACE} and TWS_{LSM} for the Niger and Zambezi basins are reflected in the NSE values (NSE: GRACE/GLDAS Niger: 0.82; Zambezi: 0.66; NSE: GRACE/CLM4.5 Niger: 0.80, Zambezi: 0.56). In the Okavango (Fig. 3c) and Limpopo (Fig. 3d) basins, TWS_{GLDAS} and TWS_{GRACE} show similarities in their patterns, but

Table 1 AAC and NSE for estimates of TWS, rainfall, temperature, and ET over the Niger, Zambezi, Okavango, and Limpopo basins

Parameter	Niger	Zambezi	Okavango	Limpopo
TWS (mm)				
AAC				
GRACE	181 ± 10	310 ± 40	134 ± 21	71 ± 26
GLDAS	135	266	126	69
CLM4.5	130	213	57	29
CLM4.5-MOD16-based	191	237	164	95
CLM4.5-FLUXNET-based	178	278	127	73
CLM4.5-GLEAM-based	180	260	113	71
NSE				
GRACE/GLDAS	0.82	0.66	0.41	0.47
GRACE/CLM4.5	0.80	0.56	0.29	0.34
GRACE/CLM4.5-MOD16-based	0.86	0.56	0.44	0.47
GRACE/CLM4.5-FLUXNET-based	0.88	0.61	0.50	0.51
GRACE/CLM4.5-GLEAM-based	0.88	0.59	0.48	0.51
Rainfall (mm/month)				
AAC				
GLDAS	152 ± 15	220 ± 28	134 ± 23	99 ± 23
CLM4.5	158 ± 12	220 ± 23	135 ± 10	104 ± 18
NSE				
GLDAS/CLM4.5	0.93	0.83	0.80	0.75
Temperature (°K)				
AAC				
CLM4.5	11 ± 0.9	7 ± 0.8	10 ± 0.8	10 ± 0.9
GLDAS	10 ± 0.9	9 ± 0.8	12 ± 1.0	10 ± 1.0
NSE				
GLDAS/CLM4.5	0.94	0.81	0.91	0.94
ET (mm/month)				
AAC				
CLM4.5	77	112	104	96
GLDAS	58	80	65	64
MOD16	45 ± 2	94 ± 7	46 ± 7	54 ± 10
GLEAM	51 ± 3	80 ± 5	75 ± 6	72 ± 7
FLUXNET	54 ± 2	70 ± 4	67 ± 5	68 ± 6
CLM4.5-MOD16-based	46	92	48	56
CLM4.5-GLEAM-based	53	79	74	69
CLM4.5-FLUXNET-based	54	70	67	68
NSE				
MOD16/CLM4.5	0.46	0.77	−0.88	−0.15
MOD16/GLDAS	0.79	0.89	0.49	0.68
GLEAM/CLM4.5	0.70	0.78	0.71	0.66
GLEAM/GLDAS	0.93	0.91	0.84	0.93
FLUXNET/CLM4.5	0.79	0.60	0.61	0.64
FLUXNET/GLDAS	0.88	0.77	0.86	0.90

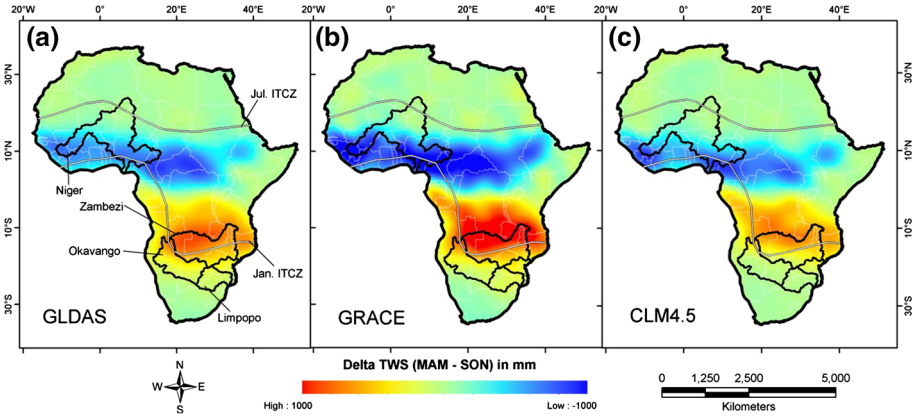

Fig. 2 Average difference in TWS (in mm) between boreal spring (March, April, May) and boreal fall (September, October, November) months extracted from **a** TWS_{GLDAS}, **b** TWS_{GRACE}, and **c** $TWS_{CLM4.5}$ over the African continent during the period from January 2003 to December 2010

differences in their amplitude which exceed TWS_{GRACE} uncertainty bounds (NSE: GRACE/GLDAS Okavango: 0.41, Limpopo: 0.47), whereas the $TWS_{CLM4.5}$ patterns and amplitude are quite different from those of TWS_{GRACE} (NSE: GRACE/CLM4.5 Okavango: 0.29, Limpopo: 0.34). For all of the examined basins, it is worth mentioning that the correspondence reflected in NSE values between the TWS_{GRACE} and TWS_{GLDAS} values is higher than that of TWS_{GRACE} and $TWS_{CLM4.5}$.

Results indicate that the CLM4.5 model underestimates the TWS amplitude of the seasonal cycle compared to modeled (TWS_{GLDAS}) and measured (TWS_{GRACE}) TWS estimates. Next, we investigate whether the observed differences in AAC, seasonality, and time series between the TWS_{GRACE} and TWS_{LSM} are related to differences in the LSMs input forcing data and/or differences in calculation schemes such as those used to estimate ET.

3.2 LSMs Forcing Precipitation (R) and Temperature (T) Data

Figure 4 shows the average annual rainfall extracted from GLDAS (R_{GLDAS}; Fig. 4a) and CLM4.5 ($R_{CLM4.5}$; Fig. 4b) forcing rainfall data over Africa. Over the African continent, areas receiving the highest amount of precipitations are those within the ITCZ (Fig. 4). The amounts and patterns of rainfall data extracted from the GLDAS and the CLM4.5 are in good agreement (Fig. 4), and so is the AAC (Table 1). For example, over the Okavango Basin the amplitude of annual cycle of rainfall (AAC) from R_{GLDAS} and $R_{CLM4.5}$ is estimated at 134 ± 23 and 135 ± 10 mm/month, respectively. Similar observations were reported for the Niger (R_{GLDAS}: 152 ± 15 mm/month; $R_{CLM4.5}$: 158 ± 12 mm/month), Zambezi (R_{GLDAS}: 220 ± 28 mm/month; $R_{CLM4.5}$: 220 ± 23 mm/month), and Limpopo (R_{GLDAS}: 99 ± 23 mm/month; $R_{CLM4.5}$: 104 ± 18 mm/month) basins.

The rainfall time series for the selected basins are displayed in Fig. 5. The NSE for the rainfall values extracted from R_{GLDAS} and $R_{CLM4.5}$ is displayed in the upper right corner in Fig. 5a–d. Examination of Fig. 5a–d shows an excellent agreement between the amplitudes, phases, and frequencies of R_{GLDAS} and $R_{CLM4.5}$; the observed differences over each of the selected basins lie mostly within the 1-sigma uncertainty limits of each estimate. The

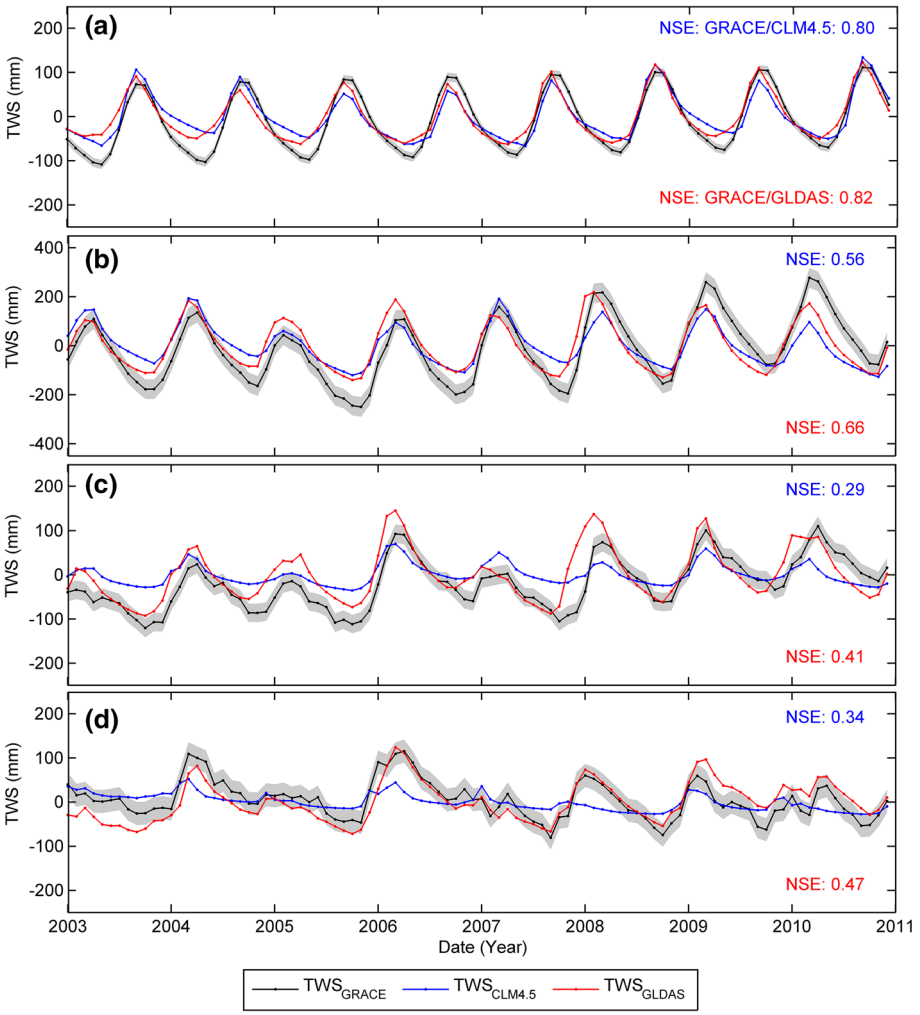

Fig. 3 Time series showing the temporal variations in monthly TWS (in mm) estimates from TWS_{GRACE} (*black line*), TWS_{GLDAS} (*red line*), and $TWS_{CLM4.5}$ (*blue line*) for the **a** Niger Basin, **b** Zambezi Basin, **c** Okavango Basin, and **d** Limpopo Basin. *Gray shading* indicates 1-sigma uncertainty limits calculated for TWS_{GRACE} data. The NSE values are displayed in the *upper right* (TWS_{GRACE}/$TWS_{CLM4.5}$; *blue text*) and the *lower right* (TWS_{GRACE}/TWS_{GLDAS}; *red text*) *corners*

correspondence between the $R_{CLM4.5}$ and R_{GLDAS} for the investigated basins is reflected in the NSE values (Niger: 0.93; Zambezi: 0.83; Okavango: 0.80; Limpopo: 0.75; Fig. 5).

Figure 6 shows the average annual air temperature extracted from GLDAS (T_{GLDAS}; Fig. 6a) and CLM4.5 ($T_{CLM4.5}$; Fig. 6b) forcing temperature data over the entire African continent. Areas affected by ITCZ are witnessing high surface temperature and excessive convection due to the heating of the Earth near the equatorial areas. In those areas, divergence currents circulate hot air away from the equator, resulting in lower surface air temperatures toward the mid-latitudes in both hemispheres (Nguyen et al. 2013). The magnitudes and patterns of air temperature data extracted from T_{GLDAS} and $T_{CLM4.5}$ are in

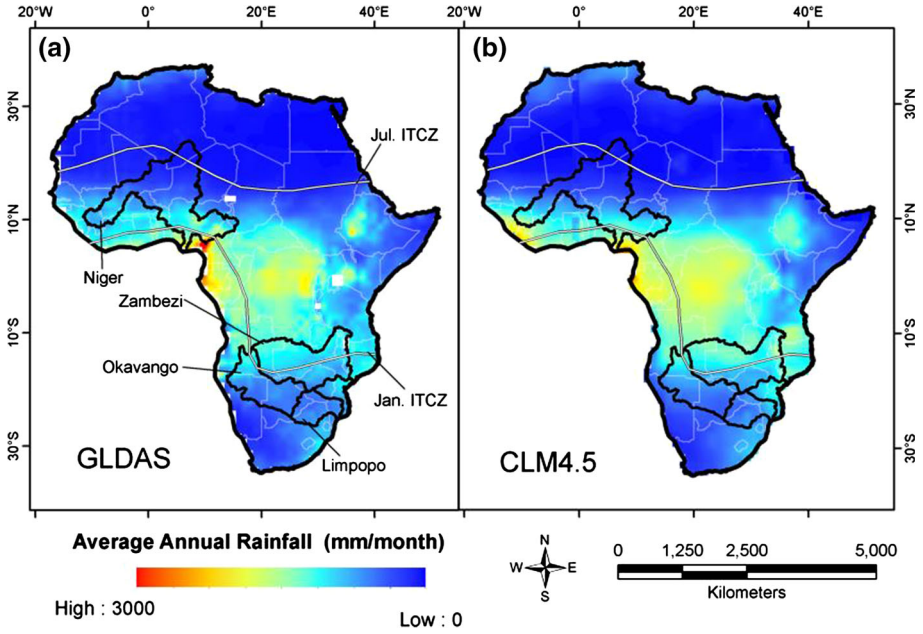

Fig. 4 Average annual rainfall (in mm/month) over the African continent extracted from **a** R_{GLDAS} and **b** $R_{CLM4.5}$ forcing rainfall data during the period from January 2003 to December 2010

good agreement (Fig. 6), and so is the AAC (Table 1) over the Limpopo ($T_{CLM4.5}$: 10 ± 0.9 °K; T_{GLDAS}: 10 ± 1.0 °K), the Zambezi ($T_{CLM4.5}$: 7 ± 0.8 °K; T_{GLDAS}: 9 ± 0.8 °K), the Okavango ($T_{CLM4.5}$: 10 ± 0.8 °K; T_{GLDAS}: 12 ± 1.0 °K), and the Niger ($T_{CLM4.5}$: 11 ± 0.9 °K; T_{GLDAS}: 10 ± 0.9 °K) basins.

The air temperature time series for the selected basins is displayed in Fig. 7. The NSE for the temperature values extracted from T_{GLDAS} and $T_{CLM4.5}$ is displayed in the upper right corner in Fig. 7a–d. Inspection of Fig. 7 shows an excellent agreement between the amplitudes, patterns, and phases of the air temperature data extracted from T_{GLDAS} and $T_{CLM4.5}$ that is reflected in the high NSE values (Niger: 0.94; Zambezi: 0.81; Okavango: 0.91; Limpopo: 0.94; Fig. 7).

Analysis of rainfall and temperature data suggests that the differences in forcing precipitation and temperature data are unlikely to be the main cause for the observed discrepancies between TWS_{GLDAS} and $TWS_{CLM4.5}$ and hence between TWS_{GRACE} and TWS_{LSM}. In the next section, we show that the differences in calculation schemes for some variables such as ET could be largely responsible for observed disagreements between TWS_{GRACE} and TWS_{LSM}.

3.3 LSMs-Derived ET

Figure 8 shows the AAC of the ET data over the African continent that was generated from the CLM4.5 ($ET_{CLM4.5}$; Fig. 8a), GLDAS (ET_{GLDAS}; Fig. 8b), FLUXNET-MTE ($ET_{FLUXNET}$; Fig. 8c), GLEAM (ET_{GLEAM}; Fig. 8d), and MOD16 (ET_{MOD16}; Fig. 8e) datasets. Inspection of Fig. 8 indicates that in general higher (lower) monthly ET values occur in wet (dry) seasons; areas witnessing higher amplitude and variability in ET are

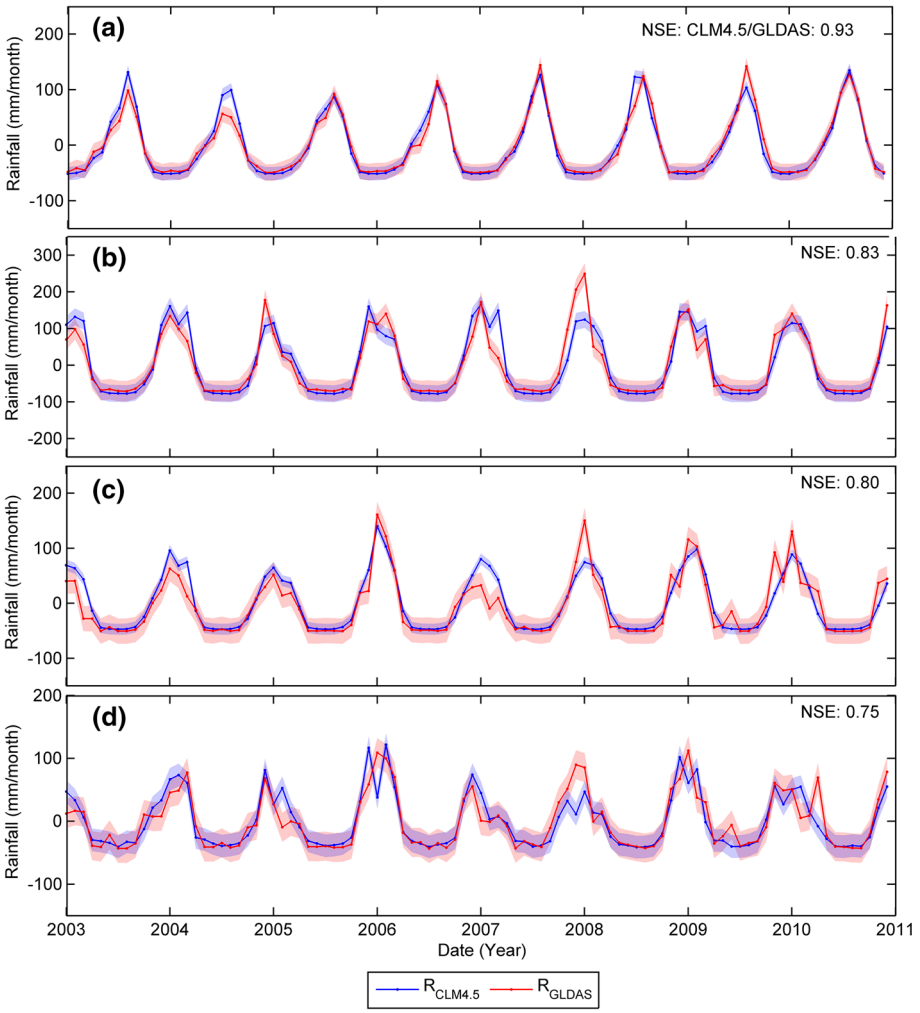

Fig. 5 Time series showing the temporal variations in monthly rainfall (in mm/month) estimates from R_{GLDAS} (*red line*) and $R_{CLM4.5}$ (*blue line*) forcing precipitation data for the **a** Niger Basin, **b** Zambezi Basin, **c** Okavango Basin, and **d** Limpopo Basin. *Blue* and *red shading* indicates 1-sigma uncertainty limits calculated for $R_{CLM4.5}$ and R_{GLDAS} data, respectively. The NSE ($R_{GLDAS}/R_{CLM4.5}$) values are displayed in the *upper right corner*

those affected by ITCZ, whereas low ET values are observed over desert regions in northern and southern Africa. Examination of Fig. 8 demonstrates that the CLM4.5 overestimates AAC of ET values compared to AAC values extracted from the other modeled (ET_{GLDAS}) and measured ($ET_{FLUXNET}$, ET_{GLEAM}, and ET_{MOD16}) estimates of ET. This could be related to differences in meteorological input data types or in retrieval algorithms and associated uncertainties used in calculating ET. The performance of a number of these methods varies from one climatic condition to another. For example, the MOD16 ET algorithm performs well over forested areas but is less adequate over arid and semiarid regions where it underestimates ET (Kim et al. 2012; Trambauer et al. 2014). It is

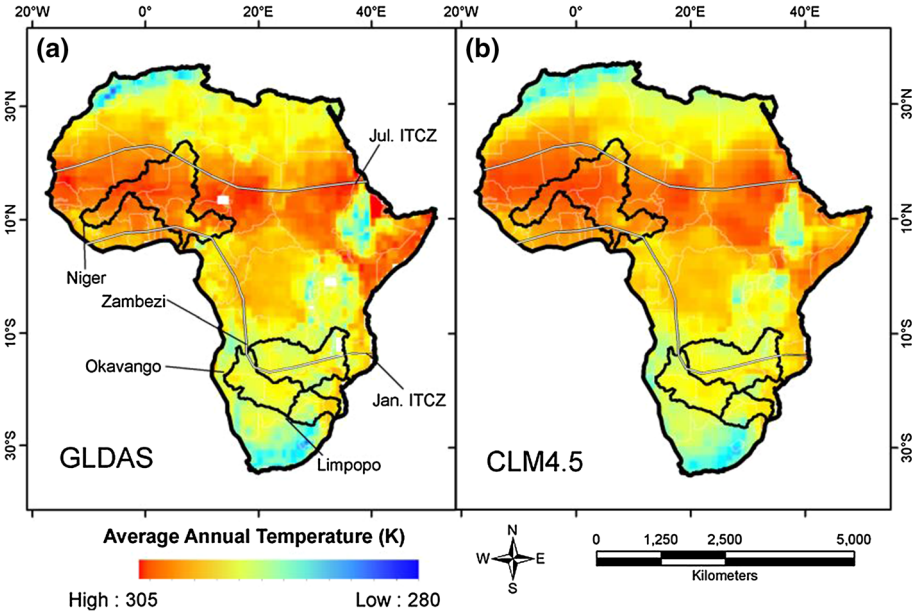

Fig. 6 Average annual air temperature (in °K) over the African continent extracted from **a** T_{GLDAS} and **b** $T_{CLM4.5}$ forcing temperature data during the period from January 2003 to December 2010

reasonable to assume that $ET_{FLUXNET}$ provides the better overall estimates for ET over Africa given that: (1) it is based on field measurements (flux tower; refer to Fig. 8c for locations), (2) $ET_{FLUXNET}$ has been traditionally used by researchers to evaluate and/or calibrate remote sensing- and LSM-based ET estimates (e.g., Fisher et al. 2008; Wanner et al. 2008; Jung et al. 2009, 2010, 2011; Beer et al. 2010; Bonan et al. 2011; Ershadi et al. 2014; Swenson and Lawrence 2014), and (3) the wide variations in climatic conditions encountered over Africa make it unlikely that any of the other $ET_{measured}$ approaches perform equally well over the entire spectrum of climatic zones within Africa.

Similar findings (CLM4.5 overestimates the AAC of ET) are observed over the investigated watersheds (Fig. 9; Table 1). In the Niger Basin, the AAC for ET from CLM4.5, GLDAS, FLUXNET, GLEAM, and MOD16 is estimated at 77, 58, 54 ± 2, 51 ± 3, and 45 ± 2 mm/month, respectively; for the Zambezi Basin they are 112, 80, 70 ± 4, 80 ± 5, and 94 ± 7 mm/month, respectively. Similarly, in the Limpopo Basin, the CLM4.5 estimates for ET are high (96 mm/month) compared to those extracted from GLDAS (64 mm/month), FLUXNET (68 ± 6 mm/month), GLEAM (72 ± 7 mm/month), and MOD16 (54 ± 10 mm/month). Comparable findings were observed over the Okavango Basin (CLM4.5: 104 mm/month, GLDAS: 65 mm/month, FLUXNET: 67 ± 5 m/month, GLEAM: 75 ± 6 mm/month, and MOD16: 46 ± 7 mm/month).

Examination of Fig. 9 shows a general agreement between the patterns and phases of $ET_{CLM4.5}$ and the remaining ET estimates; however, the CLM4.5 model overestimates ET in the summer and underestimates its values in winter months, resulting in: (1) a difference in amplitude between $ET_{CLM4.5}$ and each of the remaining ET values that exceeds the uncertainty bounds and (2) a reduction in the correspondence between the $ET_{CLM4.5}$ and each of the measured ET estimates. For example, in the Niger Basin the correspondence between

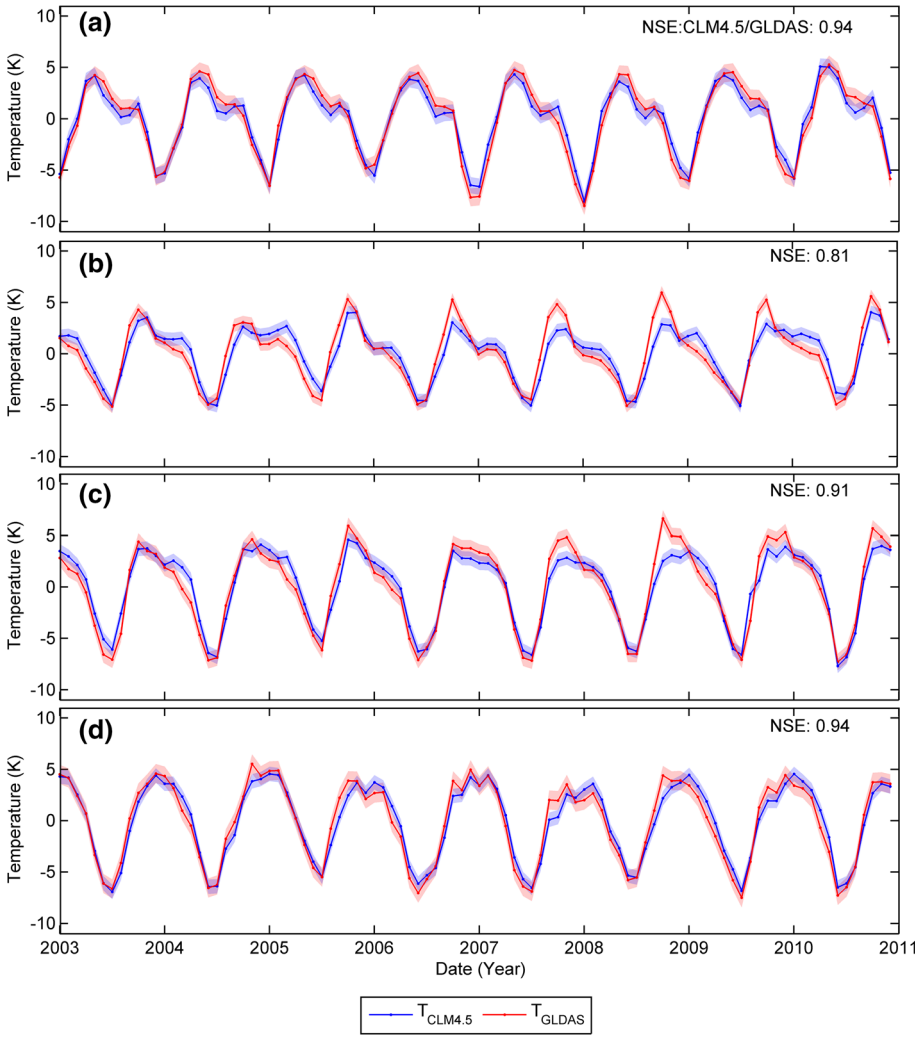

Fig. 7 Time series shows the temporal variations in monthly air temperature (in °K) estimates from T_{GLDAS} (*red line*) and $T_{CLM4.5}$ (*blue line*) forcing air surface temperature for the **a** Niger Basin, **b** Zambezi Basin, **c** Okavango Basin, and **d** Limpopo Basin. *Blue* and *red shading* indicates 1-sigma uncertainty limits calculated for $T_{CLM4.5}$ and T_{GLDAS} data, respectively. The NSE (T_{GLDAS}/$T_{CLM4.5}$) values are shown in the *upper right corner*

$ET_{CLM4.5}$ and each of ET_{MOD16}, ET_{GLEAM}, and $ET_{FLUXNET}$ is low (NSE: 0.46, 0.70, and 0.79, respectively) compared to the correspondence of ET_{GLDAS} with the $ET_{measured}$ estimates (NSE: 0.79, 0.93, and 0.88, respectively). Similar findings were observed over the Zambezi (Fig. 9b), Okavango (Fig. 9c), and Limpopo (Fig. 9d) basins (Table 1).

Our findings suggest that the ET calculation schemes for the CLM4.5 model could be largely responsible for the observed discrepancies between the $ET_{CLM4.5}$ and the measured ($ET_{FLUXNET}$, ET_{GLEAM}, and ET_{MOD16}) and modeled (ET_{GLDAS}) ET estimates. This might be largely due to the poor estimates of evaporation from the soil and transpiration from the canopy. This could result from uncertainties in parameter values; these include exposed

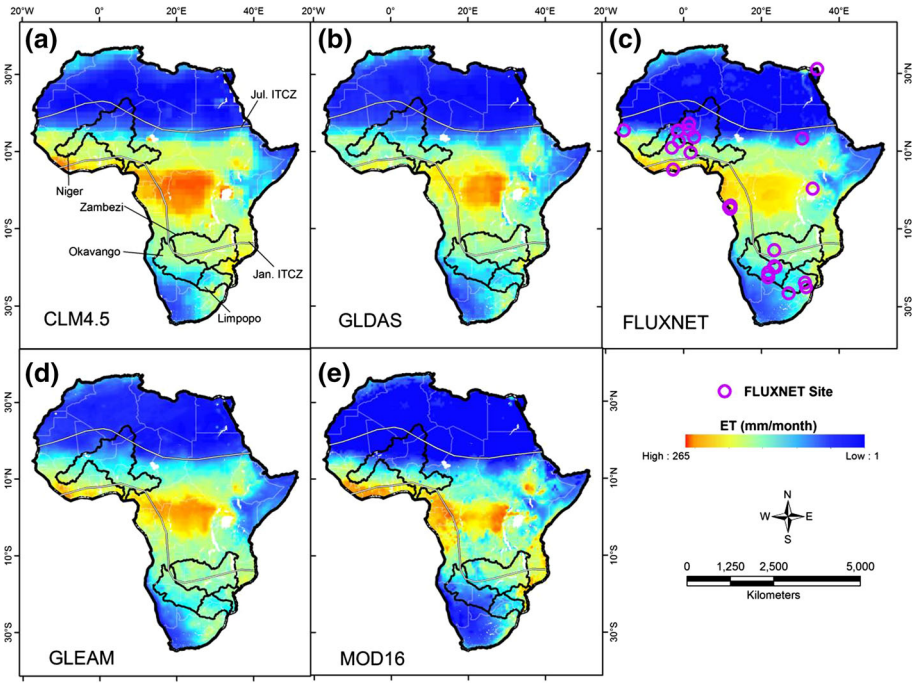

Fig. 8 Peak-to-peak AAC of ET (in mm/month) from **a** $ET_{CLM4.5}$, **b** ET_{GLDAS}, **c** $ET_{FLUXNET}$, **d** ET_{GLEAM}, and **e** ET_{MOD16} data over the African continent during the period from January 2003 to December 2010. Also shown are the locations of FLUXNET stations across Africa (**c**)

leaf and stem area indices, wet fraction of leaf and stems, and soil layer thickness. The discrepancies between $ET_{measured}$ and $ET_{CLM4.5}$ estimates could also be related to poor representation of physical process. For example, the incorporation of a dry surface soil layer to control the diffusion rate of water vapors from the soil improved the CLM4.5 outputs in semiarid region (Swenson and Lawrence 2014). Other secondary and indirect reasons for the observed disagreements between $ET_{measured}$ and $ET_{CLM4.5}$ could be related to poor model estimates of base flow, root hydraulic redistribution, and surface flow (e.g., Swenson and Lawrence 2015; Tang et al. 2015). Our findings support earlier studies that indicate that the CLM model overestimates ET and poorly simulates the partitioning of ET into soil evaporation, canopy evaporation, and transpiration (e.g., Schaefer et al. 2012; Hudiburg et al. 2013; Tang and Riley 2013; Swenson and Lawrence 2014). Next, we develop and apply first-order correction techniques to correct the bias in $ET_{CLM4.5}$ and show how those corrections can effectively adjust the TWS_{LSM}. For demonstration purposes, we apply the developed methodology to the CLM4.5-SP model outputs given the higher deviation (compared to GLDAS-Noah) from the measured TWS_{GRACE}.

4 Improving the Outputs of the CLM4.5 Model

We demonstrated that the CLM4.5 model overestimates ET in summer months and underestimates it in winter months compared to $ET_{measured}$, which in turn affects the CLM4.5-based estimates for soil moisture ($SM_{CLM4.5}$), groundwater ($GW_{CLM4.5}$), and TWS ($TWS_{CLM4.5}$).

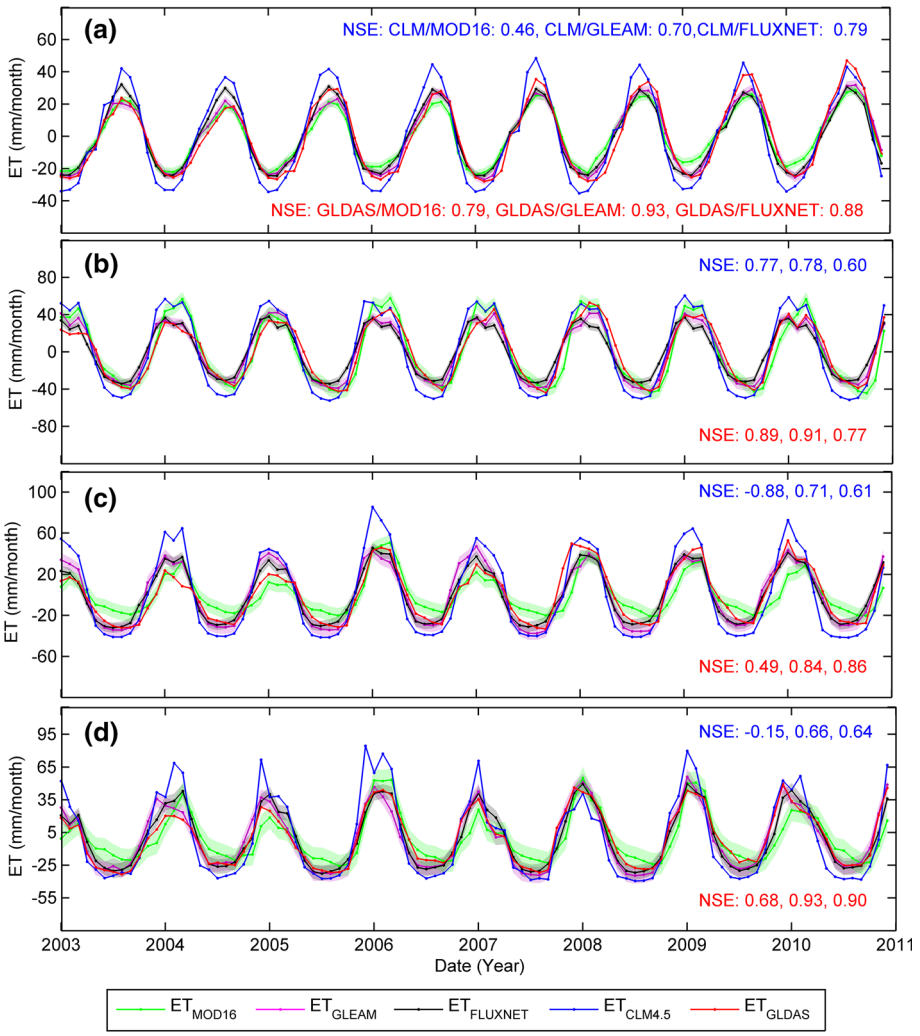

Fig. 9 Time series showing the temporal variations in monthly ET (in mm/month) estimates from $ET_{CLM4.5}$ (*blue line*), ET_{GLDAS} (*red line*), ET_{MOD16} (*green line*), ET_{GLEAM} (*magenta line*), and $ET_{FLUXNET}$ (*black line*) for the **a** Niger Basin, **b** Zambezi Basin, **c** Okavango Basin, and **d** Limpopo Basin. *Green*, *magenta*, and *gray shading* indicate 1-sigma uncertainty limits calculated for ET_{MOD16}, ET_{GLEAM}, and $ET_{FLUXNET}$ data, respectively. The NSE ($ET_{CLM4.5}/ET_{measured}$; *red text*) and ($ET_{GLDAS}/ET_{measured}$; *blue text*) values are displayed in the *upper right* and *lower right corners*, respectively

The optimum approach to address this issue is to modify the algorithm by which the CLM4.5 calculates ET. Recently, Swenson and Lawrence (2014) were able to adjust the portioning between soil evaporation and plant transpiration estimates in the CLM4.5 model over semi-arid regions in the Middle East. They attributed the bias in CLM4.5 estimates of TWS and ET to fictitious excessive soil evaporation in areas where canopy is sparse or absent, which is reducing the model estimates for moisture input into the ground. Such an approach is a step in the right direction, yet additional work is needed to refine and modify existing ET algorithms

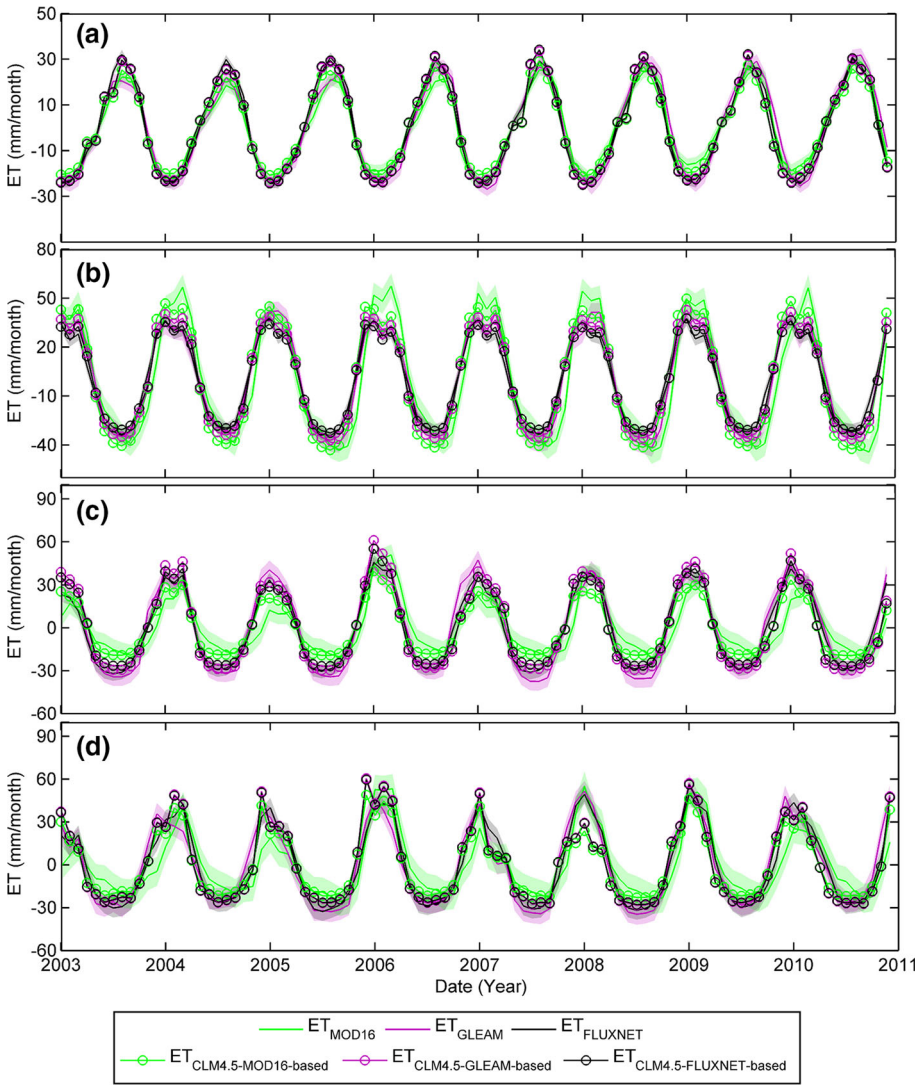

Fig. 10 Time series showing the temporal variations in monthly ET (in mm/month) estimates from MOD16 (*green line*), GLEAM (*purple line*), and FLUXNET (*black line*) data along with the corrected $ET_{CLM4.5}$ estimates based on MOD16 (*green line with circles*), GLEAM (*purple line with circles*), and FLUXNET (*black line with circles*) for the **a** Niger Basin, **b** Zambezi Basin, **c** Okavango Basin, and **d** Limpopo Basin. *Green*, *purple*, and *gray shading* indicate 1-sigma uncertainty limits calculated for MOD16, GLEAM, and FLUXNET evapotranspiration data, respectively

to minimize the bias observed in all of the remaining climatological settings and environments (e.g., temperate, tropical, and subtropical; see Sect. 5). In this study, a first-order correction technique for the $TWS_{CLM4.5}$ was developed and applied to a wide range of settings and environments across the African continent.

The adopted approach corrects $ET_{CLM4.5}$ using $ET_{measured}$ and redistributes the overestimated or underestimated amounts in $ET_{CLM4.5}$ to $SM_{CLM4.5}$ and $GW_{CLM4.5}$ estimates on

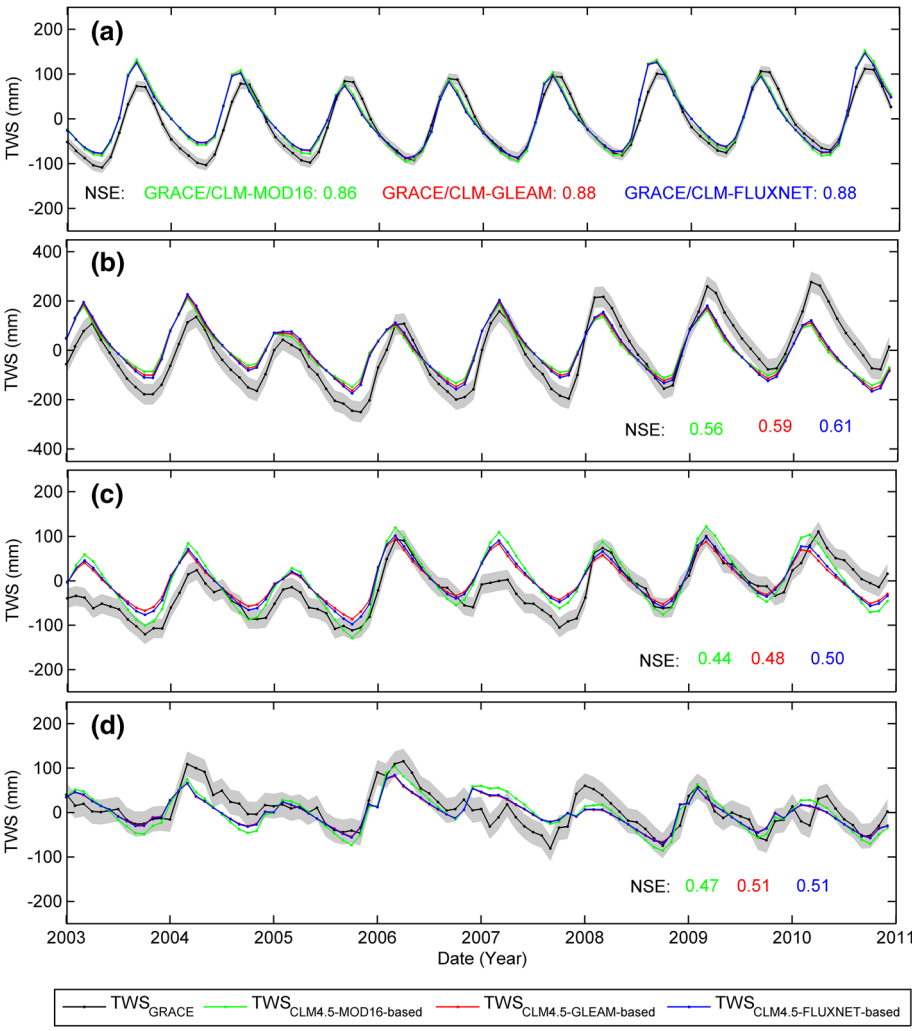

Fig. 11 Time series showing the temporal variations in monthly TWS (in mm) estimates from TWS_{GRACE} (*black line*) along with those estimated from the corrected $TWS_{CLM4.5}$ based on ET_{MOD16} (*green line*), ET_{GLEAM} (*red line*), and $ET_{FLUXNET}$ (*blue line*) for the **a** Niger Basin, **b** Zambezi Basin, **c** Okavango Basin, and **d** Limpopo Basin. *Gray shading* indicates 1-sigma uncertainty limits calculated for TWS_{GRACE}. The NSE (TWS_{GRACE}/corrected $TWS_{CLM4.5}$) values are shown in the *lower right corner* in *green* (MOD16-based correction), *red* (GLEAM-based correction), and *blue* (FLUXNET-based correction) *text*

monthly basis. Our approach improves $SM_{CLM4.5}$ and $GW_{CLM4.5}$ estimates and related processes and maintains an overall water balance within the land surface system. However, it does not estimate, nor further corrects for, potential feedbacks from the global climate model that are related to the applied ET corrections and its associated near-surface climate processes.

The following steps were conducted to remove the bias in the CLM4.5 estimates of the partitioning of precipitation into its major components: (1) $ET_{CLM4.5}$ estimates were corrected against $ET_{measured}$ estimates, (2) the difference between the original and corrected $ET_{CLM4.5}$ (hereafter referred to as excess water) was used to correct the $SM_{CLM4.5}$ and

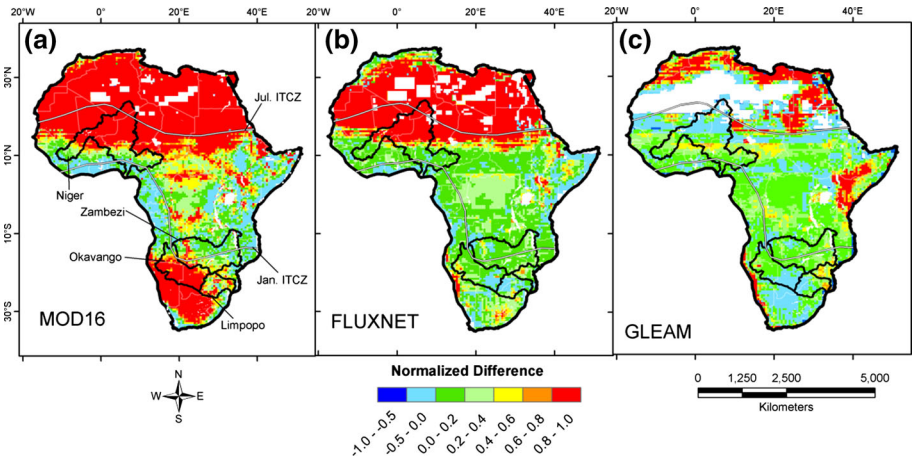

Fig. 12 Normalized difference in the AAC of **a** ET_{MOD16}, **b** $ET_{FLUXNET}$, and **c** ET_{GLEAM} over the African continent during the period from January 2003 to December 2010. Pixels with values <-1 were masked (*white polygons*)

$GW_{CLM4.5}$ by redistributing the excess water based on the ratio $\left(\theta = \frac{SM_{CLM4.5}}{GW_{CLM4.5}}\right)$, and (3) the $TWS_{CLM4.5}$ was recalculated using corrected $SM_{CLM4.5}$ and $GW_{CLM4.5}$.

Using ratios of the observed to projected standard deviations $\left(\frac{\delta_x}{\delta_{ET}}\right)$, the range of the projected $ET_{CLM4.5}$ monthly estimates was rescaled to match those of the $ET_{measured}$. The correction is implemented by applying the following equation:

$$ET(t) = \overline{ET}(t) + \left(\frac{\delta_x}{\delta_{ET}}\right) \times \left(ET_o(t) - \overline{ET}(t)\right) \tag{2}$$

where $ET_o(t)$ and $ET(t)$ are the raw and the corrected $ET_{CLM4.5}$ at a given time (t), respectively, $\overline{ET}(t)$ is the average of the $ET_{CLM4.5}$ estimates over the investigated period of January 2003 to December 2010, and δ_x and δ_{ET} are the standard deviation of the $ET_{measured}$ and $ET_{CLM4.5}$ estimates, respectively, over the investigated period. The $ET_{CLM4.5}$ estimates were corrected using each of the $ET_{measured}$ estimates one at a time.

The $SM_{CLM4.5}$ and $GW_{CLM4.5}$ estimates were then adjusted applying the following equations:

at $t = 1$:

$$SM(t) = SM_o(t) + \left(\frac{\theta(t)}{1+\theta(t)}\right) \times (ET_o(t) - ET(t)) \tag{3}$$

$$GW(t) = GW_o(t) + \left(\frac{1}{1+\theta(t)}\right) \times (ET_o(t) - ET(t)) \tag{4}$$

at $t \geq 2$:

$$SM(t) = \left(\frac{\theta(t)}{\theta(t-1)} \times \frac{1+\theta(t-1)}{1+\theta(t)}\right) \times SM(t-1) + \left(\frac{\theta(t)}{1+\theta(t)}\right) \times (R(t) - Q(t) - ET(t)) \tag{5}$$

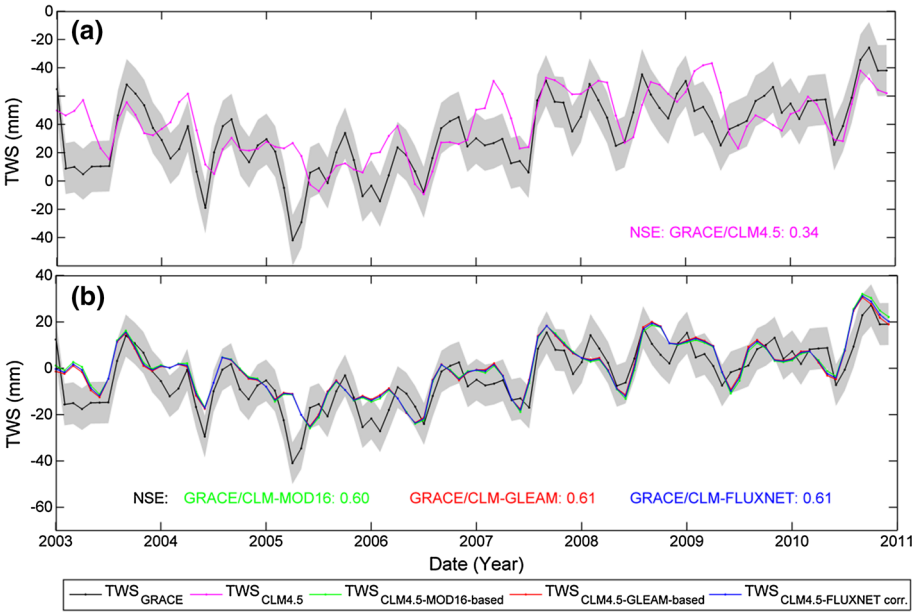

Fig. 13 Time series showing the temporal variations in monthly TWS (in mm) estimates from **a** TWS_{GRACE} (*black line*) and $TWS_{CLM4.5}$ (*magenta line*), and **b** the corrected $TWS_{CLM4.5}$ using MOD16 (*green line*), GLEAM (*red line*), and FLUXNET (*blue line*) ET estimates for the entire African continent. *Gray shading* indicates 1-sigma uncertainty limits calculated for TWS_{GRACE}. The NSE (TWS_{GRACE}, $TWS_{CLM4.5}$) value is shown in the *lower right corner* of **a** in magenta text. The NSE (TWS_{GRACE}, corrected $TWS_{CLM4.5}$) is shown in the *lower right corner* in *green* (MOD16-based), *red* (GLEAM-based), and *blue* (FLUXNET-based) *text*

$$GW(t) = \left(\frac{1+\theta(t-1)}{1+\theta(t)}\right) \times GW(t-1) + \left(\frac{1}{1+\theta(t)}\right) \times (R(t) - Q(t) - ET(t)) \quad (6)$$

where $SM(t)$ and $GW(t)$ are the corrected soil moisture and groundwater estimates of the CLM4.5 model at time (t), respectively, $SM_o(t)$ and $GW_o(t)$ are the CLM4.5 soil moisture and groundwater estimates at $t = 1$, respectively, θ is the ratio between $SM_{CLM4.5}$ and $GW_{CLM4.5}$ estimates $\left(\theta = \frac{SM_{CLM4.5}}{GW_{CLM4.5}}\right)$, and $R(t)$ and $Q(t)$ are the rainfall and runoff estimates of the CLM4.5 model, respectively. In this approach, the $SM_o(t)$ and $GW_o(t)$ values were adjusted to redistribute excess monthly water to the soil moisture $(SM(t))$ and groundwater $(GW(t))$ components in proportion to the θ value.

The corrected $TWS_{CLM4.5}$ was calculated by summing the corrected $SM_{CLM4.5}$ and $GW_{CLM4.5}$, snow, canopy storage, and channel storage in rivers for each of the examined basins. The $SM_{CLM4.5}$, $GW_{CLM4.5}$, and $TWS_{CLM4.5}$ estimates were corrected using each of the $ET_{measured}$ estimates one at a time.

The corrected $ET_{CLM4.5}$ displays patterns similar to, and fall within the 1-sigma uncertainty bounds of, the $ET_{measured}$ estimates for all of the four examined watersheds (Fig. 10). For example, the ACC of the corrected $ET_{CLM4.5}$ for the Niger Basin (MOD16-based: 46 mm/month, GLEAM-based: 53 mm/month, and FLUXNET-based: 54 mm/month; Fig. 10a; Table 1) is very close to those estimated by $ET_{measured}$ estimates (ET_{MOD16}: 45 ± 2 mm/month, ET_{GLEAM}: 51 ± 3 mm/month, and $ET_{FLUXNET}$:

54 ± 2 mm/month; Table 1). Similar findings are observed over the Zambezi (Fig. 10b), Okavango (Fig. 10c), and Limpopo (Fig. 10d) basins (Table 1).

The excess water that resulted from the ET correction was redistributed between the $SM_{CLM4.5}$ and $GW_{CLM4.5}$, given that these two components represent the bulk (in volume) of the TWS components when compared to the remaining CLM4.5 components (river channel storage, snow storages, and canopy storage); the redistribution was conducted on a monthly basis using model-based θ values for the individual months. For the investigated watersheds, the θ values were found to be <30 % (Zambezi: 0.22 ± 0.01; Limpopo: 0.26 ± 0.01; Okavango: 0.15 ± 0.01, and Niger: 0.19 ± 0.01), and their variations were found to be small (standard deviation <5 % of mean θ).

Inspection of Figs. 3a–d and 11a–d shows that the AAC of the corrected $TWS_{CLM4.5}$ for the investigated basins exceeds that of the uncorrected $TWS_{CLM4.5}$. The AAC of the corrected $TWS_{CLM4.5}$ also shows good correspondence with, and falls within the 1-sigma uncertainty range of, TWS_{GRACE}. For example, over the Limpopo Basin (Fig. 11d), the AAC of the corrected $TWS_{CLM4.5}$ increased from 29 to 95 mm (MOD16-based), 71 mm (GLEAM-based), and 73 mm (FLUXNET-based) and matches that of the TWS_{GRACE} (71 ± 26 mm; Table 1). Similar findings were observed for the Niger (Fig. 11a), Zambezi (Fig. 11b), and Okavango (Fig. 11c) basins (Table 1).

The degree to which the correction enhanced $TWS_{CLM4.5}$ estimates could be evaluated by examining the correspondence between TWS_{GRACE} and each of the uncorrected and corrected $TWS_{CLM4.5}$. If the correction resulted in higher NSE values, then this will indicate that the correspondence was enhanced and the correction was successful. In general, the corrected $TWS_{CLM4.5}$ estimates generated by using the $ET_{FLUXNET}$ in correcting $ET_{CLM4.5}$ estimates are in a better agreement (higher NSE values) with TWS_{GRACE}. This is consistent with our earlier assumption that $ET_{FLUXNET}$ provides the better overall estimates for ET over Africa. For example, in the Limpopo Basin (Fig. 11d; Table 1), the NSE increased from 0.34 (TWS_{GRACE}/$TWS_{CLM4.5}$) to 0.47 (TWS_{GRACE}/$TWS_{MOD16\text{-}based}$), 0.51 (TWS_{GRACE}/$TWS_{GLEAM\text{-}based}$), and 0.51 (TWS_{GRACE}/$TWS_{FLUXNET\text{-}based}$). Similar observations were observed for the Okavango Basin (Fig. 11c; Table 1). Similar (but of less magnitude) improvements were observed over the Niger (Fig. 11a) and Zambezi (Fig. 11b) basins (Table 1).

5 Applications and Regional Implications

Figure 12 shows the normalized difference in the AAC between $ET_{CLM4.5}$ and ET_{MODIS} ($[ET_{CLM4.5} - ET_{MOD16}]/ET_{MOD16}$; Fig. 12a), $ET_{FLUXNET}$ ($[ET_{CLM4.5} - ET_{FLUXNET}]/ET_{FLUXNET}$; Fig. 12b), and ET_{GLEAM} ($[TWS_{CLM4.5} - TWS_{GLEAM}]/ET_{GLEAM}$; Fig. 12c). Examination of Fig. 12 shows that the CLM4.5 model overestimates the AAC of ET (compared to $ET_{measured}$) for most (>85 %) of the African continent and that the degree to which the model overestimates the ET varies across the continent. For example, over the arid zones in northern and southern Africa, the CLM4.5 model overestimates ET by 80–100 % compared to ET_{MOD16} (Fig. 12a) and by ~50–60 % compared to both $ET_{FLUXNET}$ (Fig. 12b) and ET_{GLEAM} (Fig. 12c). Over the areas affected by the ITCZ, the CLM4.5 model overestimates the ET by ~40–50 % compared to ET_{MOD16} (Fig. 12a), $ET_{FLUXNET}$ (Fig. 12b) and ET_{GLEAM} (Fig. 12c). These observations indicate that $ET_{CLM4.5}$ are inaccurate over a wide range of varying climatic and hydrologic settings across the

African continent and should be adjusted so that more precise values for $SM_{CLM4.5}$, $GW_{CLM4.5}$, and $TWS_{CLM4.5}$ could be extracted.

We demonstrated that the adopted correction mechanism improves the correspondence between $TWS_{CLM4.5}$ and TWS_{GRACE} over the investigated watersheds (see Sect. 4). The question of whether the adopted algorithm can produce similar results over the entire African continent with its varied climatic settings was addressed by examining the correspondence between the TWS_{GRACE} and $TWS_{CLM4.5}$ time series before and after applying the correction.

One would expect to observe a decline in the differences in AAC values between TWS_{GRACE} and the corrected $TWS_{CLM4.5}$ and an improvement in NSE values if the correction was effective; inspection of Fig. 13a, b and Table 1 shows that this is indeed the case. Figure 13a, b shows time series for the TWS_{GRACE} and $TWS_{CLM4.5}$ over the entire African continent before and after correction, respectively. The AAC for TWS_{GRACE} (21 ± 9 mm) exceeds that extracted from $TWS_{CLM4.5}$ (16 mm) but is similar in patterns to the one extracted from the corrected $TWS_{CLM4.5}$. The AAC of the corrected $TWS_{CLM4.5}$ increased from 16 to 24 mm (MOD16-based, GLEAM-based, and FLUXNET-based) and approached that of the TWS_{GRACE} (21 ± 9 mm). The enhancement in the correspondence between the corrected $TWS_{CLM4.5}$ and the TWS_{GRACE} is reflected in the NSE values. Over the entire African continent, the NSE increased from 0.34 ($TWS_{GRACE}/TWS_{CLM4.5}$) to 0.60 (TWS_{GRACE}/TWS_{MOD16}), 0.61 (TWS_{GRACE}/TWS_{GLEAM}), and 0.61 ($TWS_{GRACE}/TWS_{FLUXNET}$).

A one-to-one correspondence between the TWS_{GRACE} and the corrected $TWS_{CLM4.5}$ time series over the entire African continent is not to be expected. Some of the observed differences displayed in Fig. 13b could be related to the fact that the CLM4.5 model is not simulating the anthropogenic contributions while GRACE is measuring both the climatic and anthropogenic effects in a given system (e.g., Lee et al. 2011; Ahmed et al. 2014; Forootan et al. 2014). Nevertheless, we demonstrated that the corrected $TWS_{CLM4.5}$ estimates over the entire African continent improved the correspondence of $TWS_{CLM4.5}$ with TWS_{GRACE} data.

The adopted approach encompassed a wide range of climatic zones including arid and hyper-arid areas in Saharan Africa, the Namibian and Kalahari deserts, semi-arid areas in the Sahel, and tropical and subtropical areas in the ITCZ zone. In the majority of these areas, it was assumed that excess water was largely partitioned in the soil moisture and groundwater storage, and not in the surface water, snow, and biomass storage compartments. While these are reasonable assumptions in the investigated areas, they are not in temperate and Arctic regions, where large portions of the hydrologic systems in these areas can be tied as snow accumulations. Similarly, in regions where river systems are prevalent, the runoff could constitute a large portion of the water budget. In such cases and settings, the correction mechanism presented in this study should be modified so that the excess water is distributed between all the significant water compartments (e.g., snow and runoff) in the investigated systems. Thus, caution should be exercised in generalizing the application of the reported correction mechanisms across all climatic and hydrologic settings. The correction algorithms (Eqs. 2–6) should be modified in accordance with the specifics of the investigated hydrologic systems.

The adopted approach has not been tested on the grid-size scale (e.g., $1^\circ \times 1^\circ$ fully distributed), yet it is here suggested that the bias applications on the basin scale remains a better option, given the added uncertainties in TWS_{GRACE} estimates (e.g., Wahr et al. 2006) and the potential for a larger anthropogenic effect on TWS_{GRACE} at these finer scales (e.g., Ahmed et al. 2014).

In this study, we concentrated our efforts on providing a demonstration for the use of TWS_{GRACE} and field measured ET for the assessment of LSMs outputs and provided straightforward techniques by which these outputs could be improved. We used the CLM4.5-SP and GLDAS-Noah models as two examples, given that they are widely used by the scientific community over the African continent. It is beyond the scope of this study to apply these methodologies to the outputs of the many other available LSMs and/or their various versions. However, our findings suggest that such efforts and applications should be conducted as they could potentially yield effective methodologies for the assessment and improvement of a wide range of LSMs outputs.

There is a growing interest in the applications of TWS_{GRACE} data to assess and improve the performance of LSMs via application of assimilation routines (e.g., Reichle et al. 2002; Walker et al. 2003; Moradkhani 2008; Zaitchik et al. 2008; Houborg et al. 2012; Eicker et al. 2014). The adopted approach should not be considered as a substitute to these efforts, yet could represent a viable alternative for the many researchers who do not have access to extensive computational resources that are needed for the assimilation of TWS_{GRACE} data into LSMs.

We use TWS_{GRACE} data to evaluate and correct outputs of LSM; the corrected TWS_{LSM}, in bulk, or separate compartments, could then be used to refine the horizontal and vertical resolution of TWS_{GRACE}. Our approach is different from those that apply scaling factors to improve the horizontal resolution of TWS_{GRACE} (e.g., Landerer and Swenson 2012). The latter involves converting the TWS_{LSM} into spherical harmonic coefficients, applying the filters used in TWS_{GRACE} data processing (e.g., destriping and Gaussian), extracting scaling factors that minimize the difference between the filtered and unfiltered TWS_{LSM} estimates, and applying these factors, in a multiplicative manner, to improve the horizontal resolution of TWS_{GRACE} (Landerer and Swenson 2012).

6 Summary

Researchers are currently taking advantage of the high vertical and spatial resolution of LSMs outputs to address the limitations in GRACE data, namely the absence of vertical resolution and its poor horizontal resolution. Such applications are compromised by the apparent inadequacies in the outputs of popular LSMs, such as the CLM4.5 model. In this study, a straightforward correction approach was developed and adopted to enhance the accuracy of the outputs of the CLM4.5 model over the entire African continent, an extensive area encompassing various climatic settings (e.g., arid, semi-arid, tropical, subtropical, Mediterranean).

Our findings indicate that the ET calculation schemes, and not the model inputs, are largely responsible for the observed discrepancies between the $ET_{CLM4.5}$ and the $ET_{measured}$. These findings are based on the following observations: (1) forcing parameters for number of LSMs were found to be similar and (2) the CLM4.5 model overestimates ET values in summer months and underestimates them in winter months compared to ET estimates extracted from field-/satellite-based ET estimates. The apparent discrepancy in $ET_{CLM4.5}$ affects the accuracy of other model outputs ($GW_{CLM4.5}$, $SM_{CLM4.5}$, and $TWS_{CLM4.5}$).

We developed and applied a straightforward correction mechanism using temporal TWS_{GRACE} measurements and field-/satellite-based ET measurements. The corrected $ET_{CLM4.5}$ estimates were then used to correct the $SM_{CLM4.5}$, $GW_{CLM4.5}$, and $TWS_{CLM4.5}$

values. The corrected $TWS_{CLM4.5}$ estimates show a better agreement (higher correlation and comparable AAC) with TWS_{GRACE}. Efforts are underway to utilize data assimilation algorithms of field- and satellite-based observations (e.g., TWS_{GRACE} and $ET_{FLUXNET}$) to improve the LSMs performance. These methods are effective, yet require computational resources that are not readily available for all researchers. The adopted correction approach could provide a viable, cost-effective, alternative for researchers that lack these resources. Our findings demonstrate the utility of TWS_{GRACE} data to calibrate the TWS_{LSM} outputs, which could in turn be used to improve the vertical and horizontal resolution of the GRACE data. Although not demonstrated in this manuscript, it is suggested that the use of corrected LSM outputs will provide more accurate results when these outputs are used to refine the vertical and horizontal resolution of TWS_{GRACE}. The launch of the GRACE-FO and GRACE-II missions will enable researchers to pursue these research directions.

Acknowledgments Funding was provided by the National Aeronautics and Space Administration (NASA) Grant NNX12AJ94G to Western Michigan University. We thank the Editor and the anonymous Reviewers of the Surveys in Geophysics for their instructive comments and suggestions.

References

Ahmed M, Sultan M, Wahr J et al (2011) Integration of GRACE (Gravity Recovery and Climate Experiment) data with traditional data sets for a better understanding of the time-dependent water partitioning in African watersheds. Geology 39:479–482. doi:10.1130/G31812.1

Ahmed M, Sultan M, Wahr J, Yan E (2014) The use of GRACE data to monitor natural and anthropogenic induced variations in water availability across Africa. Earth Sci Rev 136:289–300. doi:10.1016/j.earscirev.2014.05.009

Awange JL, Gebremichael M, Forootan E et al (2014) Characterization of Ethiopian mega hydrogeological regimes using GRACE, TRMM and GLDAS datasets. Adv Water Resour 74:64–78. doi:10.1016/j.advwatres.2014.07.012

Beer C, Reichstein M, Tomelleri E et al (2010) Terrestrial gross carbon dioxide uptake: global distribution and covariation with climate. Science 329:834–838. doi:10.1126/science.1184984

Bonan GB, Lawrence PJ, Oleson KW et al (2011) Improving canopy processes in the Community Land Model version 4 (CLM4) using global flux fields empirically inferred from FLUXNET data. J Geophys Res 116:1–22. doi:10.1029/2010JG001593

Bucchignani E, Cattaneo L, Panitz H-J, Mercogliano P (2015) Sensitivity analysis with the regional climate model COSMO-CLM over the CORDEX-MENA domain. Meteorol Atmos Phys. doi:10.1007/s00703-015-0403-3

Chen J, Li J, Zhang Z, Ni S (2014) Long-term groundwater variations in Northwest India from satellite gravity measurements. Glob Planet Change 116:130–138. doi:10.1016/j.gloplacha.2014.02.007

Dai Y, Zeng X, Dickinson RE et al (2003) The common land model. Bull Am Meteorol Soc 84:1013–1023. doi:10.1175/BAMS-84-8-1013

Döll P, Kaspar F, Lehner B (2003) A global hydrological model for deriving water availability indicators: model tuning and validation. J Hydrol 270:105–134. doi:10.1016/S0022-1694(02)00283-4

Döll P, Fritsche M, Eicker A, Müller Schmied H (2014a) Seasonal water storage variations as impacted by water abstractions: comparing the output of a global hydrological model with GRACE and GPS observations. Surv Geophys 35:1311–1331. doi:10.1007/s10712-014-9282-2

Döll P, Müller Schmied H, Schuh C et al (2014b) Global-scale assessment of groundwater depletion and related groundwater abstractions: combining hydrological modeling with information from well observations and GRACE satellites. Water Resour Res 50:5698–5720. doi:10.1002/2014WR015595

Eicker A, Schumacher M, Kusche J et al (2014) Calibration/data assimilation approach for integrating GRACE data into the WaterGAP Global Hydrology Model (WGHM) using an ensemble Kalman filter: first results. Surv Geophys 35:1285–1309. doi:10.1007/s10712-014-9309-8

Ershadi A, McCabe MF, Evans JP et al (2014) Multi-site evaluation of terrestrial evaporation models using FLUXNET data. Agric For Meteorol 187:46–61. doi:10.1016/j.agrformet.2013.11.008

Famiglietti JS, Lo M, Ho SL et al (2011) Satellites measure recent rates of groundwater depletion in California's Central Valley. Geophys Res Lett. doi:10.1029/2010GL046442

Feng W, Zhong M, Lemoine J-M et al (2013) Evaluation of groundwater depletion in North China using the Gravity Recovery and Climate Experiment (GRACE) data and ground-based measurements. Water Resour Res 49:2110–2118. doi:10.1002/wrcr.20192

Fisher JB, Tu KP, Baldocchi DD (2008) Global estimates of the land–atmosphere water flux based on monthly AVHRR and ISLSCP-II data, validated at 16 FLUXNET sites. Remote Sens Environ 112:901–919. doi:10.1016/j.rse.2007.06.025

Forman BA, Reichle RH, Rodell M (2012) Assimilation of terrestrial water storage from GRACE in a snow-dominated basin. Water Resour Res 48:W01507. doi:10.1029/2011WR011239

Forootan E, Kusche J, Loth I et al (2014) Multivariate prediction of total water storage changes over West Africa from multi-satellite data. Surv Geophys 35:913–940. doi:10.1007/s10712-014-9292-0

Gardner AS, Moholdt G, Cogley JG et al (2013) A reconciled estimate of glacier contributions to sea level rise: 2003 to 2009. Science 340:852–857. doi:10.1126/science.1234532

Gent PR, Danabasoglu G, Donner LJ et al (2011) The community climate system model version 4. J Clim 24:4973–4991. doi:10.1175/2011JCLI4083.1

Gonçalvès J, Petersen J, Deschamps P et al (2013) Quantifying the modern recharge of the "fossil" Sahara aquifers. Geophys Res Lett 40:2673–2678. doi:10.1002/grl.50478

Han S-C, Riva R, Sauber J, Okal E (2013) Source parameter inversion for recent great earthquakes from a decade-long observation of global gravity fields. J Geophys Res Solid Earth 118:1240–1267. doi:10.1002/jgrb.50116

Houborg R, Rodell M, Li B et al (2012) Drought indicators based on model-assimilated Gravity Recovery and Climate Experiment (GRACE) terrestrial water storage observations. Water Resour Res. doi:10.1029/2011WR011291

Hudiburg TW, Law BE, Thornton PE (2013) Evaluation and improvement of the Community Land Model (CLM4) in Oregon forests. Biogeosciences 10:453–470. doi:10.5194/bg-10-453-2013

Hurrell JW, Holland MM, Gent PR et al (2013) The community earth system model: a framework for collaborative research. Bull Am Meteorol Soc 94:1339–1360. doi:10.1175/BAMS-D-12-00121.1

Jacob T, Wahr J, Pfeffer WT, Swenson S (2012) Recent contributions of glaciers and ice caps to sea level rise. Nature 482:514–518. doi:10.1038/nature10847

Joodaki G, Wahr J, Swenson S (2014) Estimating the human contribution to groundwater depletion in the Middle East, from GRACE data, land surface models, and well observations. Water Resour Res 50:1–14. doi:10.1002/2013WR014633

Jung M, Reichstein M, Bondeau A (2009) Towards global empirical upscaling of FLUXNET eddy covariance observations: validation of a model tree ensemble approach using a biosphere model. Biogeosci Discuss 6:5271–5304. doi:10.5194/bgd-6-5271-2009

Jung M, Reichstein M, Ciais P et al (2010) Recent decline in the global land evapotranspiration trend due to limited moisture supply. Nature 467:951–954. doi:10.1038/nature09396

Jung M, Reichstein M, Margolis HA et al (2011) Global patterns of land–atmosphere fluxes of carbon dioxide, latent heat, and sensible heat derived from eddy covariance, satellite, and meteorological observations. J Geophys Res Biogeosci 116:1–16. doi:10.1029/2010JG001566

Kim HW, Hwang K, Mu Q et al (2012) Validation of MODIS 16 global terrestrial evapotranspiration products in various climates and land cover types in Asia. KSCE J Civ Eng 16:229–238. doi:10.1007/s12205-012-0006-1

Klees R, Zapreeva EA, Winsemius HC, Savenije HHG (2007) The bias in GRACE estimates of continental water storage variations. Hydrol Earth Syst Sci 11:1227–1241. doi:10.5194/hess-11-1227-2007

Koren V, Schaake J, Mitchell K et al (1999) A parameterization of snowpack and frozen ground intended for NCEP weather and climate models. J Geophys Res 104:19569–19585. doi:10.1029/1999JD900232

Koster RD, Suarez MJ (1996) Energy and water balance calculations in the Mosaic LSM. NASA Tech Memo 9(104606):69

Landerer FW, Swenson SC (2012) Accuracy of scaled GRACE terrestrial water storage estimates. Water Resour Res. doi:10.1029/2011WR011453

Lawrence DM, Oleson KW, Flanner MG et al (2011) Parameterization improvements and functional and structural advances in version 4 of the Community Land Model. J Adv Model Earth Syst 3:1–27. doi:10.1029/2011MS000045

Lawrence DM, Oleson KW, Flanner MG et al (2012) The CCSM4 land simulation, 1850–2005: assessment of surface climate and new capabilities. J Clim 25:2240–2260. doi:10.1175/JCLI-D-11-00103.1

Lee H, Beighley RE, Alsdorf D et al (2011) Characterization of terrestrial water dynamics in the Congo Basin using GRACE and satellite radar altimetry. Remote Sens Environ 115:3530–3538. doi:10.1016/j.rse.2011.08.015

Lenk O (2013) Satellite based estimates of terrestrial water storage variations in Turkey. J Geodyn 67:106–110. doi:10.1016/j.jog.2012.04.010

Levin NE, Zipser EJ, Ceding TE (2009) Isotopic composition of waters from Ethiopia and Kenya: insights into moisture sources for eastern Africa. J Geophys Res Atmos 114:1–13. doi:10.1029/2009JD012166
Li BL, Rodell M, Zaitchik BF et al (2012) Assimilation of GRACE terrestrial water storage into a land surface model: evaluation and potential value for drought monitoring in western and central Europe. J Hydrol 446–447:103–115. doi:10.1016/j.jhydrol.2012.04.035
Liang X, Lettenmaier DP, Wood EF (1996) One-dimensional statistical dynamic representation of subgrid spatial variability of precipitation in the two-layer variable infiltration capacity model. J Geophys Res 101:21403. doi:10.1029/96JD01448
Long D, Longuevergne L, Scanlon BR (2015) Global analysis of approaches for deriving total water storage changes from GRACE satellites. Water Resour Res 51:2574–2594. doi:10.1002/2014WR016853
Miralles DG, Gash JH, Holmes TRH et al (2010) Global canopy interception from satellite observations. J Geophys Res Atmos 115:1–8. doi:10.1029/2009JD013530
Miralles DG, De Jeu RAM, Gash JH et al (2011a) Magnitude and variability of land evaporation and its components at the global scale. Hydrol Earth Syst Sci 15:967–981. doi:10.5194/hess-15-967-2011
Miralles DG, Holmes TRH, De Jeu RAM et al (2011b) Global land-surface evaporation estimated from satellite-based observations. Hydrol Earth Syst Sci 15:453–469. doi:10.5194/hess-15-453-2011
Moradkhani H (2008) Hydrologic remote sensing and land surface data assimilation. Sensors 8:2986–3004. doi:10.3390/s8052986
Mu Q, Heinsch FA, Zhao M, Running SW (2007) Development of a global evapotranspiration algorithm based on MODIS and global meteorology data. Remote Sens Environ 111:519–536
Mu Q, Zhao M, Running SW (2011) Improvements to a MODIS global terrestrial evapotranspiration algorithm. Remote Sens Environ 115:1781–1800. doi:10.1016/j.rse.2011.02.019
Nash JE, Sutcliffe JV (1970) River flow forecasting through conceptual models, part I—a discussion of principles. J Hydrol 10:282–290
Nguyen H, Evans A, Lucas C et al (2013) The Hadley circulation in reanalyses: climatology, variability, and change. J Clim 26:3357–3376. doi:10.1175/JCLI-D-12-00224.1
Niu G-Y, Yang Z-L (2006) Assessing a land surface model's improvements with GRACE estimates. Geophys Res Lett 33:L07401. doi:10.1029/2005GL025555
Oleson KW, Lawrence DM, Gordon B et al (2010) Technical description of version 4.0 of the Community Land Model (CLM). NCAR Tech Note Note NCAR/TN-478+STR, 257
Reichle R, McLaughlin DB, Entekhabi D (2002) Hydrologic data assimilation with the ensemble Kalman filter. Mon Weather Rev 130:103–114. doi:10.1175/1520-0493(2002)130<0103:HDAWTE>2.0.CO;2
Rodell M, Houser PR, Jambor U et al (2004) The global land data assimilation system. Bull Am Meteorol Soc 85:381–394. doi:10.1175/BAMS-85-3-381
Rodell M, Velicogna I, Famiglietti JS (2009) Satellite-based estimates of groundwater depletion in India. Nature 460:999–1002. doi:10.1038/nature08238
Scanlon BR, Longuevergne L, Long D (2012) Ground referencing GRACE satellite estimates of groundwater storage changes in the California Central Valley, USA. Water Resour Res. doi:10.1029/2011WR011312
Schaefer K, Schwalm CR, Williams C et al (2012) A model-data comparison of gross primary productivity: results from the North American Carbon Program site synthesis. J Geophys Res Biogeosci 117:1–15. doi:10.1029/2012JG001960
Steffen H, Wu P (2011) Glacial isostatic adjustment in Fennoscandia—a review of data and modeling. J Geodyn 52:169–204. doi:10.1016/j.jog.2011.03.002
Su H, Yang Z-L, Dickinson RE et al (2010) Multisensor snow data assimilation at the continental scale: the value of Gravity Recovery and Climate Experiment terrestrial water storage information. J Geophys Res 115:D10104. doi:10.1029/2009JD013035
Sultan M, Ahmed M, Sturchio N et al (2013) Assessment of the Vulnerabilities of the Nubian Sandstone Fossil Aquifer, North Africa. In: Pielke RA, Hossain F (eds) Climate vulnerability: understanding and addressing threats to essential resources. Elsevier Inc., Academic Press, Amsterdam, pp 311–333
Sultan M, Ahmed M, Wahr J et al (2015) Monitoring aquifer depletion from space: case studies from the Saharan and Arabian Aquifers. In: Lakshmi V (ed) Remote sensing of the terrestrial water cycle, AGU geophysical monograph 206, pp 349–366
Swenson SC, Lawrence DM (2014) Assessing a dry surface layer-based soil resistance parameterization for the Community Land Model using GRACE and FLUXNET-MTE data. J Geophys Res 119:10299–10312. doi:10.1002/2014JD022314
Swenson SC, Lawrence DM (2015) A GRACE-based assessment of interannual groundwater dynamics in the Community Land Model. Water Resour Res 51:8817–8833. doi:10.1002/2014WR016259
Swenson S, Wahr J (2006) Post-processing removal of correlated errors in GRACE data. Geophys Res Lett 33:L08402. doi:10.1029/2005GL025285

Tang J, Riley WJ (2013) Impacts of a new bare-soil evaporation formulation on site, regional, and global surface energy and water budgets in CLM4. J Adv Model Earth Syst 5:558–571. doi:10.1002/jame.20034

Tang J, Riley WJ, Niu J (2015) Incorporating root hydraulic redistribution in CLM4.5: effects on predicted site and global evapotranspiration, soil moisture, and water storage. J Adv Model Earth. doi:10.1002/2015MS000484

Tapley BD, Bettadpur S, Ries JC et al (2004) GRACE measurements of mass variability in the Earth system. Science 305:503–505. doi:10.1126/science.1099192

Tiwari VM, Wahr J, Swenson S (2009) Dwindling groundwater resources in northern India, from satellite gravity observations. Geophys Res Lett 36:L18401. doi:10.1029/2009GL039401

Trambauer P, Dutra E, Maskey S et al (2014) Comparison of different evaporation estimates over the African continent. Hydrol Earth Syst Sci 18:193–212. doi:10.5194/hess-18-193-2014

Velicogna I, Wahr J (2013) Time-variable gravity observations of ice sheet mass balance: precision and limitations of the GRACE satellite data. Geophys Res Lett 40:3055–3063. doi:10.1002/grl.50527

Velicogna I, Sutterley TC, Broeke MR Van Den (2014) Regional acceleration in ice mass loss from Greenland and Antarctica using GRACE time-variable gravity data. Geophys Res Lett 41:8130–8137. doi:10.1002/2014GL061052

Viovy N, Ciais P (2015) CRUNCEP data set for 1901–2008. http://dods.extra.cea.fr/data/p529viov/cruncep/. Accessed Oct 2015

Voss KA, Famiglietti JS, Lo M et al (2013) Groundwater depletion in the Middle East from GRACE with implications for transboundary water management in the Tigris–Euphrates–Western Iran region. Water Resour Res 49:904–914. doi:10.1002/wrcr.20078

Wahr JM (2007) Time variable gravity from satellites. Treatise Geophys 3:213–237. doi:10.1016/B978-044452748-6.00176-0

Wahr J, Molenaar M, Bryan F (1998) Time variability of the Earth's gravity field: hydrological and oceanic effects and their possible detection using GRACE. J Geophys Res 103:30205–30229. doi:10.1029/98JB02844

Wahr J, Swenson S, Zlotnicki V, Velicogna I (2004) Time-variable gravity from GRACE: first results. Geophys Res Lett 31:20–23. doi:10.1029/2004GL019779

Wahr J, Swenson S, Velicogna I (2006) Accuracy of GRACE mass estimates. Geophys Res Lett 33:L06401. doi:10.1029/2005GL025305

Walker JP, Houser PR, Reichle RH (2003) New technologies require advances in hydrologic data assimilation. Eos (Washington DC) 84:545–551. doi:10.11029/2002/WRR001545

Wanner H, Beer J, Bütikofer J et al (2008) Mid-to late Holocene climate change: an overview. Quat Sci Rev 27:1791–1828. doi:10.1016/j.quascirev.2008.06.013

Werth S, Güntner A (2009) Calibration analysis for water storage variability of the global hydrological model WGHM. Hydrol Earth Syst Sci Discuss 6:4813–4861. doi:10.5194/hessd-6-4813-2009

Werth S, Güntner A, Petrovic S, Schmidt R (2009) Integration of GRACE mass variations into a global hydrological model. Earth Planet Sci Lett 277:166–173. doi:10.1016/j.epsl.2008.10.021

Widiastuti E (2009) Data assimilation of GRACE terrestrial water storage data into a hydrological model using the ensemble Kalman smoother: a case study of the Rhine river basin. Masters Thesis, Civil Engineering and Geosciences, TU Delft, 74 p

Wouters B, Bonin JA, Chambers DP et al (2014) GRACE, time-varying gravity Earth system dynamics and climate change. Rep Prog Phys. doi:10.1088/0034-4885/77/11/116801

Xie P, Arkin PA (1997) Global precipitation: a 17-year monthly analysis based on gauge observations, satellite estimates, and numerical model outputs. Bull Am Meteorol Soc 78:2539–2558. doi:10.1175/1520-0477(1997)078<2539:GPAYMA>2.0.CO;2

Zaitchik BF, Rodell M, Reichle RH (2008) Assimilation of GRACE terrestrial water storage data into a land surface model: results for the Mississippi River Basin. J Hydrometeorol 9:535–548. doi:10.1175/2007JHM951.1